iScience

CellPress
OPEN ACCESS

Article

Increased cardiac PFK-2 protects against high-fat diet-induced cardiomyopathy and mediates beneficial systemic metabolic effects

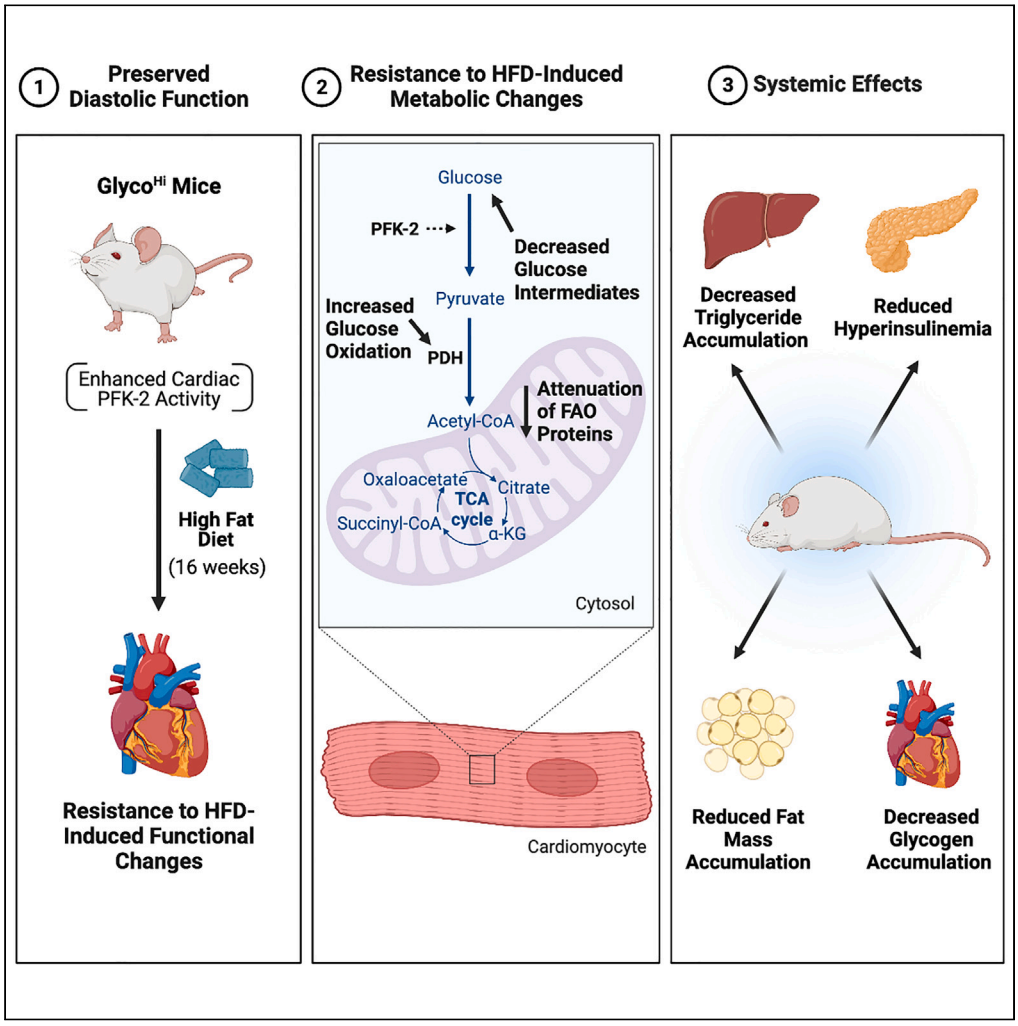

Maria F. Mendez Garcia, Satoshi Matsuzaki, Albert Batushansky, ..., Ying Ann Chiao, Michael Kinter, Kenneth M. Humphries

kenneth-humphries@omrf.org

Highlights

Normalizing cardiac metabolism may relieve cardiometabolic syndrome

Increasing cardiac glycolysis prevents high-fat diet-induced diastolic dysfunction

Cardiac mitochondrial function, proteomics, and metabolomics are normalized under HFD

Increasing cardiac glycolysis showed systemic resistance to the harmful effects of HFD

Mendez Garcia et al., iScience 26, 107131
July 21, 2023
https://doi.org/10.1016/j.isci.2023.107131

iScience

CellPress
OPEN ACCESS

Article

Increased cardiac PFK-2 protects against high-fat diet-induced cardiomyopathy and mediates beneficial systemic metabolic effects

Maria F. Mendez Garcia,[1,2] Satoshi Matsuzaki,[1] Albert Batushansky,[1,4] Ryan Newhardt,[1] Caroline Kinter,[1] Yan Jin,[3] Shivani N. Mann,[2] Michael B. Stout,[1] Haiwei Gu,[3] Ying Ann Chiao,[1] Michael Kinter,[1] and Kenneth M. Humphries[1,2,5,*]

SUMMARY

A healthy heart adapts to changes in nutrient availability and energy demands. In metabolic diseases like type 2 diabetes (T2D), increased reliance on fatty acids for energy production contributes to mitochondrial dysfunction and cardiomyopathy. A principal regulator of cardiac metabolism is 6-phosphofructo-2-kinase/fructose-2,6-bisphosphatase (PFK-2), which is a central driver of glycolysis. We hypothesized that increasing PFK-2 activity could mitigate cardiac dysfunction induced by high-fat diet (HFD). Wild type (WT) and cardiac-specific transgenic mice expressing PFK-2 (Glyco^{Hi}) were fed a low fat or HFD for 16 weeks to induce metabolic dysfunction. Metabolic phenotypes were determined by measuring mitochondrial bioenergetics and performing targeted quantitative proteomic and metabolomic analysis. Increasing cardiac PFK-2 had beneficial effects on cardiac and mitochondrial function. Unexpectedly, Glyco^{Hi} mice also exhibited sex-dependent systemic protection from HFD, including increased glucose homeostasis. These findings support improving glycolysis via PFK-2 activity can mitigate mitochondrial and functional changes that occur with metabolic syndrome.

INTRODUCTION

Diabetic cardiomyopathy (DCM) is defined as cardiomyopathy developed in the presence of diabetes but without conditions such as hypertension and coronary artery disease.[1] DCM distinctively presents as left ventricular hypertrophy and reduced diastolic function. Due to the overlap between obesity, insulin resistance, and diabetes, individuals with metabolic syndrome develop similar cardiomyopathies, even in the absence of diabetes.[2,3] Diastolic dysfunction and pathological hypertension are reversible in the early stages of metabolic syndrome, emphasizing the need for the development of effective interventions.[4]

The heart has incessant energy requirements, yet it has a limited capacity to store nutrients.[5] The heart must therefore continuously adapt to changes in nutrient availability to meet dynamic energetic demands. The healthy heart primarily uses fatty acid oxidation (FAO) as the major source of energy production (40–90%) but can switch to carbohydrate metabolism (10–50%) in response to insulin and hormonal signals.[6,7] With the occurrence of metabolic syndrome, the heart is exposed to excessive levels of fatty acids and carbohydrates. High-circulating lipids and impaired insulin signaling prevent proper glucose uptake and metabolism, leading to a state of metabolic inflexibility in which the heart relies increasingly more on FAO for energy production.[8] In addition, excess nutrient levels may lead to an accumulation of metabolic intermediates and lipotoxicity.[3,9]

There are no therapeutics that directly normalize cardiac metabolism, but the key regulatory points that control glucose metabolism are logical targets. In glycolysis, phosphofructokinase-1 (PFK-1) catalyzes the first irreversible and rate-limiting step. Given its central importance, the regulation of PFK-1 is dynamic; being inhibited by cytosolic citrate and ATP levels and activated by fructose 2,6-bisphosphate (Fru-2,6-P_2) and ADP. Fru-2,6-P_2 is a potent allosteric activator of PFK-1 that is produced and degraded by the bifunctional enzyme phosphofructokinase-2/fructose bisphosphatase-2 (PFK-2, in this work).[10,11] The cardiac PFK-2 production of Fru-2,6-P_2 is increased during insulin and β-adrenergic signaling.[12,13] Additionally,

[1]Aging and Metabolism Research Program, Oklahoma Medical Research Foundation, Oklahoma City, OK, USA

[2]Department of Biochemistry and Molecular Biology, University of Oklahoma Health Sciences Center, Oklahoma City, OK, USA

[3]Center for Translational Science, Florida International University, Port St. Lucie, FL, USA

[4]Ilse Katz Institute for Nanoscale Science & Technology, Ben-Gurion University of the Negev, Beer Sheva, Israel

[5]Lead contact

*Correspondence: kenneth-humphries@omrf.org

https://doi.org/10.1016/j.isci.2023.107131

the activation of PFK-2 is sufficient to increase glucose oxidation even in the presence of fatty acids.[11] Our laboratory has previously shown that PFK-2 levels decrease under diabetic conditions, implicating its loss of content and activity as a driver of metabolic inflexibility.[14]

In addition to the PFK-1/PFK-2 regulatory nexus, mitochondrial-localized pyruvate dehydrogenase (PDH) and pyruvate dehydrogenase kinase 4 (PDK4) regulate glucose oxidation.[15] PDH converts pyruvate to acetyl-CoA and consequently plays a central role in metabolic fuel selection. PDK4 phosphorylates and inhibits PDH, decreasing glucose oxidation under conditions such as fasting or HFD, where FAO is further elevated.[16,17] Thus, the cellular energy sensing systems of cytosolic PFK-1/PFK-2 and mitochondrial PDH/PDK4 work together to sustain metabolic flexibility through the dynamic coordination of cardiac macronutrient metabolism.

We previously sought to examine how sustaining cardiac PFK-2 activity, when challenged with short-term metabolic stress, affects metabolism and mitochondrial function. To do so, we employed studies on Glyco^{Hi} mice that express a constitutively active form of PFK-2 that increases Fru-2,6-P_2 and enhances glycolysis, regardless of normal physiological stimuli.[18,19] We found that Fru-2,6-P_2 levels are sustained in Glyco^{Hi} mice under low-insulin conditions (i.e., fasting and HFD) and that Glyco^{Hi} mice have a unique metabolic profile in response to a 1-week HFD treatment.[19,20] Compared to WT, Glyco^{Hi} hearts had increased proteins involved in glycolysis and decreased early glycolytic intermediates. In addition, this previous study also led to the discovery of a mechanism where levels of cytosolic Fru-2,6-P_2 increased mitochondrial PDK4 in a secondary adaptive response to prevent excess pyruvate oxidation.[20]

The present study focused on investigating the potential beneficial effects of sustained glycolysis in the context of HFD-induced cardiomyopathy, which develops under chronic metabolic stress conditions. To do so, we implemented long-term nutrient stress with a 16-week HFD treatment. Cardiac function, mitochondrial bioenergetics, and proteomic and metabolomic profiles were evaluated in WT and Glyco^{Hi} mice. We report that Glyco^{Hi} hearts were protected from an HFD-induced decrease to diastolic function. Glyco^{Hi} mitochondria had dampened HFD-induced functional changes compared to WT. In agreement with our functional data, proteomic and metabolomic analyses revealed Glyco^{Hi} hearts had an overall diminished response to HFD-mediated metabolic reprogramming. Unexpectedly, we also found that Glyco^{Hi} mice have a systemic resistance to some of the deleterious, whole-body effects of HFD such as increased serum insulin levels. Our results demonstrate that improved metabolic balance between glucose oxidation and fatty acid oxidation can result in beneficial effects on cardiac and mitochondrial function.

RESULTS

Wild type and Glyco^{Hi} mice have comparable weight gain in 16-week HFD treatment

Increasing cardiac glycolysis may mitigate obesity-induced disruption of cardiac metabolism and function. To test this possibility, we placed wild type (WT) and Glyco^{Hi} mice on HFD treatment for 16 weeks to induce obesity and promote an increase in cardiac fatty acid oxidation. Control groups were placed on an LFD. Both male and female Glyco^{Hi} mice gained weight on the HFD similarly as compared to WT mice (Figures S1A–S1D). Quantitative magnetic resonance (QMR) was used as a noninvasive method for measuring body composition. Analysis of fat and lean mass revealed a diet-dependent gain in percent fat mass and loss of percent lean mass in male mice, regardless of genotype (Figures S1E and S1F). Similar diet-dependent changes to fat and lean mass were also seen in female WT and Glyco^{Hi} mice, although Glyco^{Hi} mice displayed a slightly abated gain in percent fat mass and loss of percent lean mass (Figures S1G and S1H).

Cardiac function is preserved in Glyco^{Hi} hearts under high-fat diet conditions

Diastolic dysfunction is a key characteristic of metabolic cardiomyopathies like DCM. Long-term HFD treatment can induce this pathology in mice.[21] Echocardiography analysis performed on a subset of male mice after 16 weeks of HFD treatment revealed a diet-induced decrease in the ratio of early to late diastolic mitral annulus velocities (Ea/Aa), indicating a diminished diastolic function in WT hearts. Remarkably, this decrease in diastolic function was absent in Glyco^{Hi} mice on HFD (Figure 1A; Table S1). No reduction in systolic function, measured as fractional shortening or ejection fraction was observed in any experimental group (Figures 1B and 1C). Hypertrophy and left ventricular concentric remodeling are also commonly seen in metabolic cardiomyopathies. However, when assessing the heart weight of all male mice used in this study, hypertrophy was absent in WT hearts. Glyco^{Hi} mice did have a 14% increase in heart

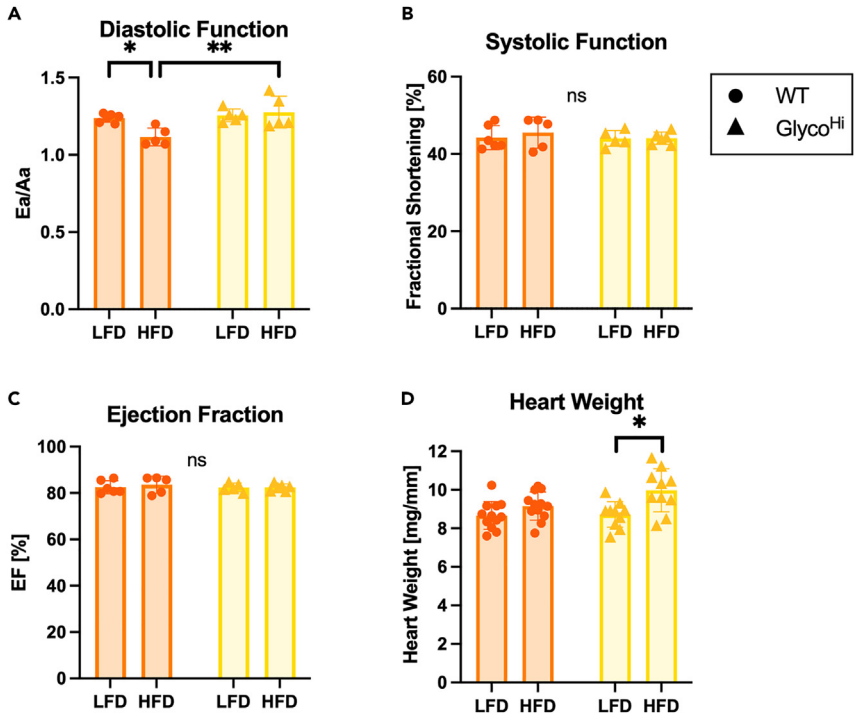

Figure 1. Cardiac function is preserved in Glyco^{Hi} hearts under high-fat diet conditions

Male WT and Glyco^{Hi} were fed a 16-week low-fat diet (LFD) or high-fat diet (HFD) and cardiac function was assessed by echocardiography.

(A) Diastolic function (Ea/Aa) of male hearts.

(B) Systolic function of male hearts measured as fractional shortening (%).

(C) Ejection fraction (%) of male heart (A–C) WT/LFD n = 6, WT/HFD n = 5; Glyco^{Hi}/LFD n = 5, Glyco^{Hi}/HFD n = 6).

(D) Male heart weight normalized to tibia length (mg/mm) (n = 12 per WT group; n = 10 per Glyco^{Hi} group). Scatterplot data are represented as the mean ± SD. *$p < 0.05$, **$p < 0.01$, by two-way ANOVA with Tukey multiple comparisons test. Data points represent individual biological replicates. See also Table S1 and Figure S2.

mass with HFD treatment, but because they have preserved diastolic and systolic functions, the slight hypertrophy was non-pathological (Figure 1D).

Echocardiography data indicated a diet-dependent increase in concentric remodeling, regardless of genotype by two-way ANOVA (Figure S2). Global cardiac dysfunction can be assessed through the myocardial performance index (MPI), which incorporates both systolic and diastolic functions. Interestingly, Glyco^{Hi}/HFD also had a trend toward lower (better) MPI value compared to WT/HFD (Figure S2), further indicating Glyco^{Hi} mice have conserved cardiac function under HFD conditions, compared to WT. Taken together, these data signify that increased cardiac PFK-2 activity preserves diastolic function under HFD conditions.

Glyco^{Hi} cardiac mitochondria have attenuated functional alterations in response to HFD

The ability of mitochondria to metabolize different nutrients is an essential aspect of metabolic flexibility and overall cardiac health. HFD causes metabolic remodeling, characterized by increased reliance on fatty acids for energy production, and contributes to the occurrence and progression of diabetic cardiomyopathy.[22] We sought to determine if the enhanced cardiac PFK-2 activity of Glyco^{Hi} mice helps to sustain mitochondrial pyruvate oxidation under HFD conditions. In isolated heart mitochondria, we measured state 3 respiration (ADP-dependent maximal respiration) using two primary energy substrates, pyruvate or palmitoyl-carnitine (PC). Pyruvate was used as the glycolytic substrate and PC as the fatty acid substrate. The ratio of PC-supported state 3 to pyruvate-supported state 3 respiration [state 3 respiration ratio = PC/pyruvate respiration rates] can be used to assess mitochondrial substrate preference and also provides a means of analysis that minimizes day-to-day variability. We have previously reported that the ratio of PC- to pyruvate-supported respiration is lower basally in Glyco^{Hi} mitochondria compared to WT on a normal chow diet.[20]

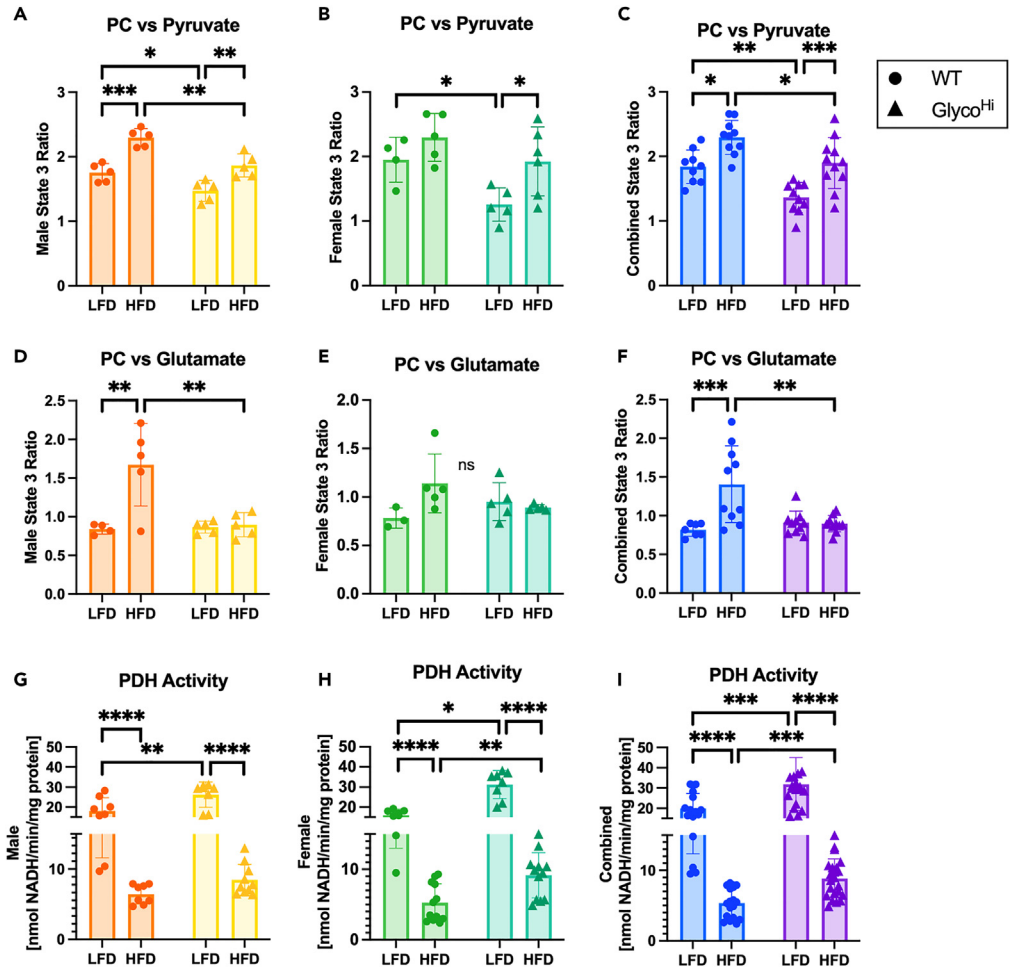

Figure 2. Glyco^{Hi} cardiac mitochondria have attenuated functional alterations in response to HFD

Male and female WT and Glyco^{Hi} were fed a 16-week low-fat diet (LFD) or high-fat diet (HFD). Following cardiac mitochondria isolation, state 3 respiration was measured using either pyruvate, PC, or glutamate and PDH activity was measured by a spectrophotometer-based assay.

(A) Male PC vs. pyruvate state 3 respiration ratios (n = 5 per group).

(B) Female PC vs. pyruvate state 3 respiration ratios (n = 5 per WT group; Glyco^{Hi}/LFD n = 5, Glyco^{Hi}/HFD n = 6).

(C) Combined PC vs. pyruvate state 3 respiration ratios.

(D) Male PC vs. glutamate state 3 respiration ratios (WT/LFD n = 4, WT/HFD n = 5; n = 5 per Glyco^{Hi} group).

(E) Female PC vs. glutamate state 3 respiration (WT/LFD n = 3, WT/HFD n = 5; Glyco^{Hi} n = 5 per group).

(F) Combined PC vs. glutamate state 3 respiration ratios.

(G) Male PDH activity (WT n = 4; per group; Glyco^{Hi}/LFD n = 4, Glyco^{Hi}/HFD n = 5).

(H) Female PDH activity (WT/LFD n = 4, WT/HFD n = 6; Glyco^{Hi}/LFD n = 4, Glyco^{Hi}/HFD n = 6). (I) Combined PDH activity.

Data points represent individual biological replicates. PDH activity data is also represented with technical duplicates. Scatterplot data are represented as the mean ± SD. *p < 0.05, **p < 0.01, ***p < 0.001 ****p < 0.0001 by two-way ANOVA with Tukey multiple comparisons test. See also Table S2 and Figure S3.

This indicates maximal oxidative phosphorylation rates are relatively greater with pyruvate in Glyco^{Hi} mitochondria as compared to WT.

In this study, mitochondrial respiration analysis determined that the ratio of PC-supported to pyruvate-supported respiration is lower in Glyco^{Hi}/LFD vs. WT/LFD in both males (1.47 ± 0.16; 1.71 ± 0.15, respectively) and females (1.26 ± 0.26; 1.95 ± 0.35, respectively) (Figures 2A–2C). This result, consistent with our previous report,[20] indicates increased pyruvate oxidation in Glyco^{Hi} hearts, relative to WT. After 16 weeks, WT male mice on HFD had a significant increase in the PC/pyruvate ratio (2.29 ± 0.13) driven by increased PC-supported respiration, indicating an adaptation that facilitates augmented mitochondrial FAO

(Figure 2A). The PC/pyruvate ratio also increased in the Glyco^{Hi}/HFD group (1.86 ± 0.17) but remained lower than in WT/HFD mice. Uniquely, the increase was driven primarily by decreased pyruvate respiration, not by an increase in PC respiration as in WT (Figure 2A; Table S2). Notably, though, the Glyco^{Hi}/HFD groups still sustained higher pyruvate-supported respiration rates than WT/HFD groups (Table S2). The abated increase in the PC/pyruvate ratio in the Glyco^{Hi}/HFD group points to a reduced diet-induced reliance on fatty acid utilization compared to WT mitochondria. A similar response to HFD treatment was seen in female WT (2.30 ± 0.37) and Glyco^{Hi} (1.92 ± 0.53) mitochondria, and analysis of a combination of both sexes illustrates the relative resistance of Glyco^{Hi} mitochondria to HFD-induced changes to substrate utilization (Figures 2B and 2C).

Glutamate-supported respiration is routinely used with isolated mitochondria as a means of evaluating maximal NADH-linked respiration.[23] Here, we identified a marked difference in the glutamate-supported respiration profiles of Glyco^{Hi} mitochondria. Male WT mitochondria had an increase in the ratio of PC to glutamate state 3 respiration in response to HFD (LFD = 0.85 ± 0.07; HFD = 1.67 ± 0.53). In contrast, the ratio remained unchanged in Glyco^{Hi} mitochondria (LFD = 0.87 ± 0.08; HFD = 0.90 ± 0.16) (Figure 2D). Female mitochondria differed from males and did not have significant diet-induced changes in their PC/glutamate ratios for both WT (LFD = 0.78 ± 0.1; HFD = 1.14 ± 0.3) and Glyco^{Hi} (LFD = 0.95 ± 0.19; HFD = 0.89 ± 0.03), although a significant interaction effect was identified by two-way ANOVA (Figure 2E). Combining the male and female data revealed a significant genotypic effect, diet, and interaction effect by two-way ANOVA (Figure 2F). Individual mitochondrial parameters also revealed specific sex and genotype deviations in mitochondrial response to nutrients (Table S2). Notably, the respiratory control ratios (RCR) of male and female Glyco^{Hi} mitochondria were less sensitive to HFD-diet treatment compared to WT. Mitochondria from WT/HFD groups had overall reduced RCR values with all three substrates, indicating decreased respiration efficiency. Together these data show Glyco^{Hi} mitochondria retain more stabilized mitochondrial respiration under HFD conditions.

Pyruvate dehydrogenase (PDH) is a primary point of metabolic regulation because its activity controls the overall rate of glucose oxidation. Assessment of PDH activity thus provides further information about cardiac glucose consumption. PDH activity was significantly increased in Glyco^{Hi}/LFD compared to WT/LFD, in both males (26.2 ± 6.3; 18.15 ± 6.54, respectively) and females (31.26 ± 6.93; 16.01 ± 3.02, respectively) (Figures 2G–2I). This is consistent with an increased rate of glucose oxidation in Glyco^{Hi} mitochondria. Although HFD decreased both WT and Glyco^{Hi} PDH activities, male Glyco^{Hi}/HFD (8.47 ± 2.21) trended toward increased PDH activity compared to WT/HFD (6.44 ± 1.39), and this genotypic difference was seen more distinctly in female Glyco^{Hi} hearts (9.17 ± 3.2) compared to WT (5.26 ± 2.69) on HFD (Figures 2G and 2H). When sexes were combined, Glyco^{Hi} mitochondria had significantly higher rates of PDH activity compared to their WT/LFD and HFD counterparts (Figure 2I). In agreement with the changes to activity, phosphorylation of PDH was also decreased in Glyco^{Hi} hearts compared to WT with a more distinctive effect seen in females (Figures S3A–S3C). This further supports that Glyco^{Hi} mitochondria retain a greater capacity for glucose oxidation under HFD conditions. To investigate the differences in PDH activity, PDK4 and, lon protease protein levels were assessed. PDK4 phosphorylates (inhibits) PDH while lon protease specifically and rapidly degrades PDK4.[24] PDK4 levels increased similarly in HFD-treated groups (Figure S3D). Interestingly, lon protease levels increased robustly only in Glyco^{Hi}/HFD. This suggests that PDK4 may be more rapidly degraded in Glyco^{Hi} hearts, as compared to WT/HFD, and this could contribute to increased PDH activity.

Carnitine palmitoyltransferase I (CPT1) catalyzes the first step in the transfer of long-chained fatty acids from the cytosol into the mitochondrial intermembrane space.[25] Changes in its activity indicate alterations in the capacity of mitochondria to take up and oxidize fatty acids. In males, CPT1 activity increased in a diet-dependent manner regardless of genotype but was lower in Glyco^{Hi}/LFD compared to WT/LFD. In females, a diet effect was detected by two-way ANOVA with no significant changes within the groups (Figures S3F–S3H). CPT1 activity is regulated by the allosteric inhibitor, malonyl-CoA, that is produced by acetyl-CoA carboxylase (ACC). ACC activity is regulated by inhibitory phosphorylation which can serve as a proxy for its activity. In males, phospho-ACC was similar between all groups although expression of total ACC was increased in Glyco^{Hi}/HFD (Figures S3I and S3J). In contrast, females showed a marked decrease in phospho-ACC in WT/HFD compared to WT/LFD (Figures S3K and S3L). This suggests Glyco^{Hi} heart mitochondria do not have impaired CPT1 activity, but its regulation by malonyl-CoA likely differs between genotypes and sex.

We also investigated whether there were any genotypic or diet-induced effects on electron transport chain (ETC) activities and mitochondrial content. NADH oxidase activity, a measurement of total ETC, was slightly decreased in Glyco^{Hi} vs. WT, with a genotype effect identified by two-way ANOVA. There was no significant HFD-induced change in activity in either WT or Glyco^{Hi} groups (Figures S3M–S3O). Complex I activity, the rate-limiting step of the ETC, showed a similar trend as NADH oxidase, which had a significant genotype effect by two-way ANOVA (Figures S3P–S3R). To assess changes to mitochondrial content, proteins from complexes I, II, IV, and ATP synthase were quantified. The results show that on LFD, Glyco^{Hi} hearts have decreased mitochondrial proteins compared to WT/LFD. However, in response to HFD, Glyco^{Hi} (but not WT) increased mitochondrial protein content. This effect was slightly different between sexes but with similar trends (Figures S3S and S3T). These results provide evidence that there are bioenergetic differences between Glyco^{Hi} and WT hearts and that each genotype adapts to the HFD stress through unique mechanisms.

Glyco^{Hi} mice display mitigated diet-induced alterations to cardiac proteome

We next measured how Glyco^{Hi} hearts differed in their global metabolic response to HFD through a targeted proteomic analysis. Male and female hearts were analyzed, and the obtained results were first subjected to a cluster analysis. Subsequently, a pathway analysis was performed on the proteins in each distinct cluster. The top primary metabolic pathway(s) uniquely changed in each cluster that were chosen and are listed with their relative magnitude of change in Figure 3. Cluster and pathway analysis revealed an overall similar pattern of change between males and females, with some discrete differences found in females.

Clusters I in both sexes are comprised of proteins that had increased relative abundance in response to HFD (Figures 3A and 3B). Pathway analysis identified fatty acid metabolism as a top pathway in both males and females, with thermogenesis as an additional pathway in males. Proteins separated into clusters II had a combined diet and genotype effect. WT/HFD groups had a robust relative increase of tricarboxylic acid cycle (TCA) proteins. In contrast, the Glyco^{Hi}/LFD group had a lower abundance of these proteins and an attenuated increase in response to HFD. This could be attributed, in part, to lower mitochondrial protein abundance in Glyco^{Hi}/LFD. Additional pathways identified in clusters II include peroxisome in males, and fatty-acid metabolism and branched-chain amino acid (BCAA) metabolism in females, which were lower in Glyco^{Hi}/HFD groups compared to WT. Proteins in clusters III had unique changes ascribed specifically to genotype. In general, changes to protein abundance in response to HFD in clusters III were opposite between WT and Glyco^{Hi} groups. Glycolysis/gluconeogenesis was the primary pathway shared between males and females in clusters III. WT groups had a greater abundance of these glycolytic proteins with HFD treatment. These proteins had an overall lower abundance in Glyco^{Hi} groups compared to WT. Lastly, cluster analysis assigned female data into a fourth, unique cluster. Cluster IV had a combined genotype and diet effect that was distinct from the combined effect seen in cluster III (Figure 3B). This can be seen in the WT/LFD group going from red, in cluster III, to blue in cluster IV with the top metabolic pathways being amino acid metabolism, glycolysis/gluconeogenesis, and HIF-1 signaling.

Interestingly, pathway analysis found the pentose phosphate pathway and fructose/mannose metabolism, non-primary metabolic pathways associated with obesity and diabetes, uniquely changed in males (cluster III) and females (clusters III/IV). Proteins involved in these pathways were more abundant in WT/HFD groups and were generally lower in Glyco^{Hi}. Overall, cluster and pathway analysis data are consistent with our mitochondrial function results that showed WT/HFD groups had increased PC/pyruvate ratios primarily driven by augmented lipid-supported respiration, which agrees with the increased abundance to FAO proteins in clusters I (Figures 3A and 3B). In Glyco^{Hi} groups, cluster analysis revealed a marked decrease in glycolysis proteins. Functionally, this corresponds with the increased PC/pyruvate respiratory (Figures 2A–2C) ratio being driven primarily by decreased pyruvate-supported respiration and not by increased reliance on PC.

Cellular stress responses to HFD differ between WT and Glyco^{Hi} hearts

The cluster analysis provided an unbiased means of determining pathways that were affected by genotype and/or diet. We also directly analyzed the alterations to individual proteins, including antioxidants and other proteins related to lipotoxicity, that are well-established for their roles in oxidative stress and obesity-related cardiomyopathies (Figures 4, and S4). Previous studies have found proteins such as the cluster of differentiation 36 (CD36), the heart-type fatty acid-binding protein (Fabp3), and the adipocyte-type fatty acid-binding protein (Fabp4) play a role in the development of lipotoxicity in DCM.[26,27] In the heart, CD36 is a key transporter of long-chain fatty acids across the cell membrane. Fabp3 and Fabp4

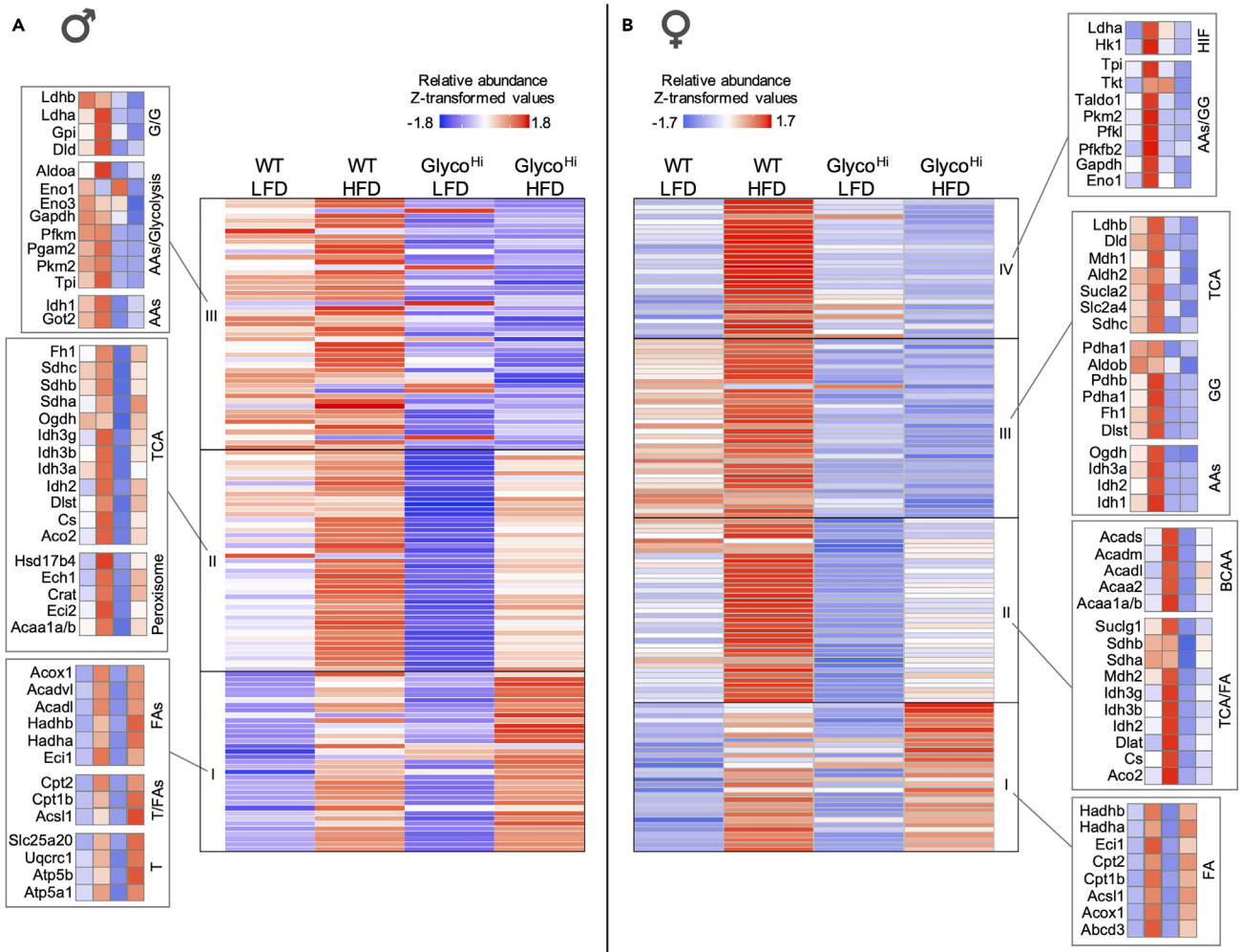

Cluster number	Metabolic pathway	Direction of change			
		WT LFD	WT HFD	Glyco^Hi LFD	Glyco^Hi HFD
I	Fatty acid metabolism Thermogenesis	↓	↑	↓	↑
II	TCA cycle Peroxisome	↔	↑↑	↓↓	↔
III	Glycolysis/Gluconeogenesis Amino acid metabolism	↑	↑	↓	↓

Cluster number	Metabolic pathway	Direction of change			
		WT LFD	WT HFD	Glyco^Hi LFD	Glyco^Hi HFD
I	Fatty acid metabolism	↓	↑	↓	↑
II	TCA cycle Fatty acids metabolism BCAA metabolism	↔	↑↑	↓↓	↔
III	TCA cycle Glycolysis / Gluconeogenesis Biosynthesis of amino acids	↑	↑↑	↓	↓
IV	Amino Acid metabolism Glycolysis / Gluconeogenesis HIF-1 signaling	↓	↑↑	↓	↓

Figure 3. Glyco^Hi mice display mitigated diet-induced alterations to cardiac proteome

Male and female WT and Glyco^Hi were fed a 16-week low-fat diet (LFD) or high-fat diet (HFD). Heatmap representation of metabolic proteins measured in total heart homogenates of male (A) and female (B) mice by selected reaction monitoring mass spectrometry (Male WT/LFD n = 5, WT/HFD n = 4; Glyco^Hi n = 5 per group) (Female WT/LFD n = 5, WT/HFD n = 6; Glyco^Hi/LFD n = 5, Glyco^Hi/HFD n = 6). Cluster numbers are labeled I-IV on the heatmap. *Below heatmap*, list of the major pathway(s) unique to each cluster with the directionality of change to the proteins involved in the pathway. [↓ = relative decrease, ↓↓ = strong relative decrease, ↑ = relative increase, ↑↑ = strong relative increase, ↔ = no relative change]. AAs = Amino acid metabolism, BCAA = Branched-chain amino acid, FAs/FA = Fatty acid metabolism, G/G = Glycolysis/Gluconeogenesis, T = Thermogenesis, TCA = Tricarboxylic acid. See also Figures S7–S16.

are lipid chaperones involved in the intracellular trafficking of long-chain fatty acids into mitochondria. Protein expression of CD36, Fabp3, and Fabp4 increased in WT groups in response to HFD but retained lower expression in all Glyco^Hi groups (Figure 4). Further inspection of individual enzymes revealed an abated

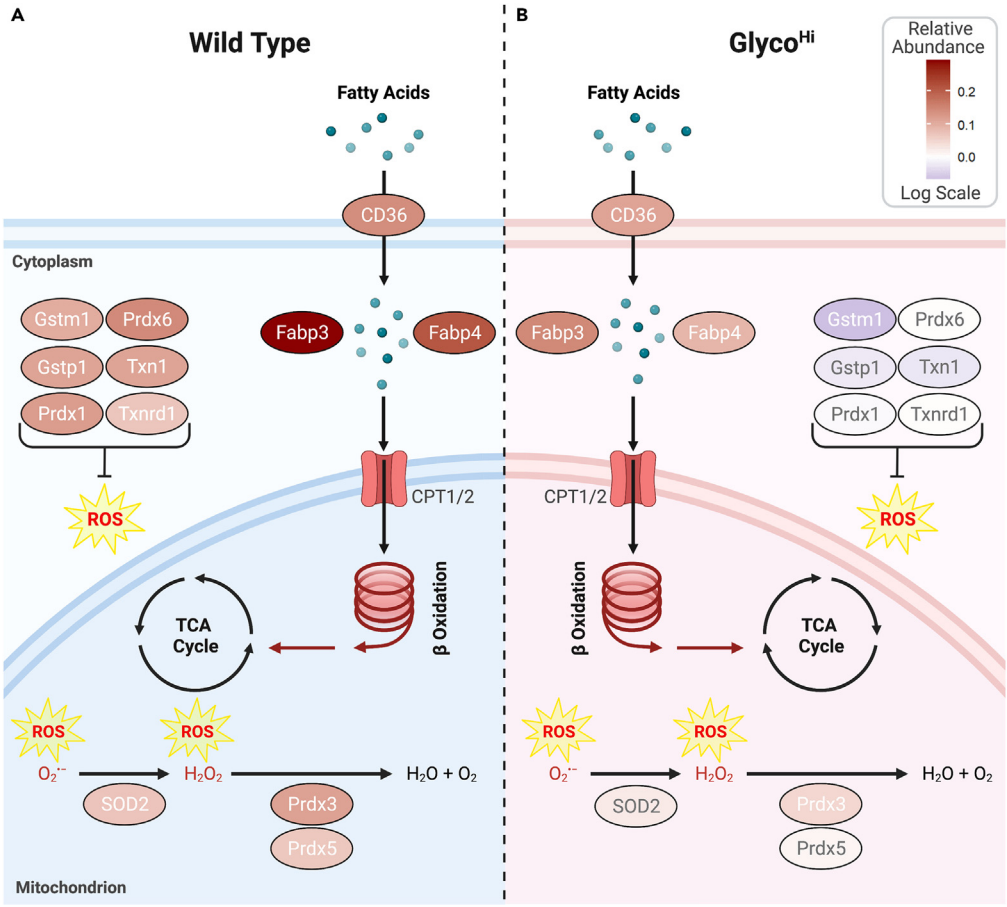

Figure 4. Cellular stress responses to HFD differ between WT and Glyco^{Hi} hearts

Fatty acid transport and antioxidant proteins were measured in total heart homogenates by selected reaction monitoring mass spectrometry. Combined male and female data are represented by the *false color heatmap* of the -fold changes under HFD conditions (Males: WT/LFD n = 5, WT/HFD n = 4; n = 5 per Glyco^{Hi} group) (Females: WT/LFD n = 5, WT/HFD n = 6; Glyco^{Hi}/LFD n = 5, Glyco^{Hi}/HFD n = 6).

(A) Effect of diet on protein expression in WT (HFD/LFD) hearts.

(B) Diet effect on protein expression and Glyco^{Hi} (HFD/LFD) hearts. Data are -fold change of means in log10 scale. ROS = Reactive Oxygen Species. See also Figure S4.

HFD-induced increase of FAO proteins in male and female Glyco^{Hi} hearts compared to WT by two-way ANOVA (Figures S9 and S10).

Chronic HFD leads to hyperinsulinemia (quantified below in Figure 7I) and Akt activation. Akt activation has numerous downstream effects on metabolism, including the translocation of CD36 that contributes to lipotoxicity.[28] In WT hearts, total Akt content decreased but phosphorylation (activation) was significantly increased in response to HFD (Figures S4M and S4N). Akt phosphorylation also increased in Glyco^{Hi} groups. However, Glyco^{Hi} hearts had genotype-dependent lower levels of phosphorylation (Figures S4M and S4N). This supports that Glyco^{Hi} hearts are less affected by hyperinsulinemia in response to chronic HFD as compared to WT.

In metabolic cardiomyopathies like DCM, metabolic alterations such as augmented FAO and mitochondrial dysfunction increase reactive oxygen species (ROS) and activate the cellular antioxidant defense system. Cytosolic antioxidant proteins, peroxiredoxin 1 and 6 (Prdx1, Prdx6), were elevated in WT/HFD groups but remained unchanged in Glyco^{Hi} groups. Mitochondrial Prdx3 was increased in WT/HFD groups and both Prdx3 and Prdx5 had higher expression in WT groups compared to Glyco^{Hi}. Other antioxidant proteins (SOD2, Gstm1, Gstp1, Txn1, Txnrd1) were also elevated only in WT hearts following HFD treatment (Figures 4 and S4).

We next measured protein carbonylation, a marker of oxidative stress, in total heart tissue. WT hearts had greater protein carbonylation than Glyco^{Hi} hearts under LFD conditions (Figure S4O). Unexpectedly, WT hearts had decreased protein carbonylation with HFD treatment (Figure S4O). The decrease in protein carbonylation may be explained by the increase in antioxidant defense proteins. In contrast, Glyco^{Hi} heart protein carbonylation was unaffected by diet. Together, these findings provide evidence that Glyco^{Hi}/HFD hearts have an attenuated increase in FAO proteins, a concurrent abated response in the antioxidant defense enzymes, and a lower occurrence of protein carbonylation.

Metabolic profiling reveals fewer HFD-induced changes in Glyco^{Hi} hearts

The metabolomic analysis provides a direct functional report of the physiological state of a system and has become a powerful tool in the study of T2D both in basic science and clinical settings. Semitargeted LC-MS analysis in both positive and negative modes was performed separately and 160 (95 and 65 respectively) metabolites were identified. The normalized and filtered data were subjected to two-way ANOVA analysis to identify changes in metabolites in response to diet, sex, or a diet-sex effect. The results, visualized by Venn diagram, determined that Glyco^{Hi} hearts had generally fewer significantly altered metabolites as compared to WT hearts (Figure S5A). To further evaluate global metabolic changes, principal component analysis (PCA) was performed on WT and Glyco^{Hi} HFD-treated groups. PCA plots of both positive and negative modes revealed a strong genotype effect on metabolism under HFD conditions (Figures S5B and S5C). Interestingly, a strong sex effect was also seen in metabolites measured in positive mode (Figure S5B).

The cardiac structural and metabolic remodeling that occurs in metabolic diseases like T2D results in a buildup of lipid, carbohydrate, and amino acid metabolites.[29–33] Inspection of these individual metabolites showed a diminished accumulation in Glyco^{Hi} groups (Figure 5). For example, glucose and lactate levels were elevated in WT compared to Glyco^{Hi} groups. The lower abundance of lactate in Glyco^{Hi} hearts is consistent with proteomic results showing that protein levels of the heart-type lactate dehydrogenase (Ldhb) are also lower in Glyco^{Hi} hearts compared to WT (Figures S7 and S8). Although lactate was significantly reduced in Glyco^{Hi} hearts, alanine levels increased in Glyco^{Hi}/HFD-treated groups. This could represent an HFD-associated conversion of pyruvate or glutamate to alanine (Figure 5). Likewise, oxaloacetate is also increased in Glyco^{Hi} hearts compared to WT and increases further in response to HFD (Figure 5). Metabolites involved in ancillary glycolysis pathways such as ribose-5-phosphate (R5P), sorbitol, mannose, and UDP-GlcNAc had lower abundance in Glyco^{Hi} groups compared to WT (Figure 5). These findings are also in agreement with proteomic results. Specifically, pathway analysis revealed the pentose phosphate and fructose/mannose metabolism pathways were only elevated WT groups (Figure 4). Additionally, proteomics analysis showed that protein levels of aldose reductase (Akr1b1) were lower in Glyco^{Hi} groups compared to WT, and this is supported by metabolomic results showing sorbitol, the product of aldose reductase, is also less abundant in Glyco^{Hi} hearts (Figures S11 and S12).

Closer inspection of metabolites with known disease associations further illustrated genotypic differences. Other metabolites involved in ancillary glycolysis pathways such as glucose-1-phosphate (G-1-P), serine, and glycine had a unique genotype and/or diet effect. Although G-1-P was increased in WT/HFD vs. WT/LFD, only Glyco^{Hi}/LFD had a distinct increase in G-1-P compared. Glyco^{Hi} hearts exhibited elevated serine and glycine levels in an HFD-dependent and genotype-dependent manner, respectively (Figure 5). Branched-chain amino acids (BCAAs) leucine and isoleucine had a diet-dependent increase in WT/HFD groups. In contrast, Glyco^{Hi} hearts did not have a significant change to BCAAs in response to HFD. Metabolite levels of BCAAs are also consistent with proteomic pathway analysis results which identified the BCAA pathway proteins being elevated in female (Figure 3B) and male (Figure S9) WT hearts. To investigate if the HFD-increase of BCAAs in WT groups was sufficient to activate mTORC1 signaling (a master senor of nutrient and energy),[34,35] the phosphorylation levels of its substrate 4E-BP1 were measured. Although total 4E-BP1 levels were significantly higher in Glyco^{Hi} hearts compared to WT, the phosphorylation levels were lower. This supports mTORC1 is not hyperactivated in WT hearts. Lastly, heptadecanoic acid, which is reduced in T2D, decreased in WT/HFD vs. WT/LFD but remained unchanged in Glyco^{Hi} groups.[31] Together, metabolomic results indicate that Glyco^{Hi} hearts have diminished HFD changes to several metabolic markers associated with metabolic dysfunction and T2D.

Whole-body metabolism varies between WT and Glyco^{Hi} mice

Long-term HFD causes increased organ weight due to the accumulation of excess fat storage. Examination of individual tissue weights uncovered unanticipated systemic effects brought on by the cardiac-specific

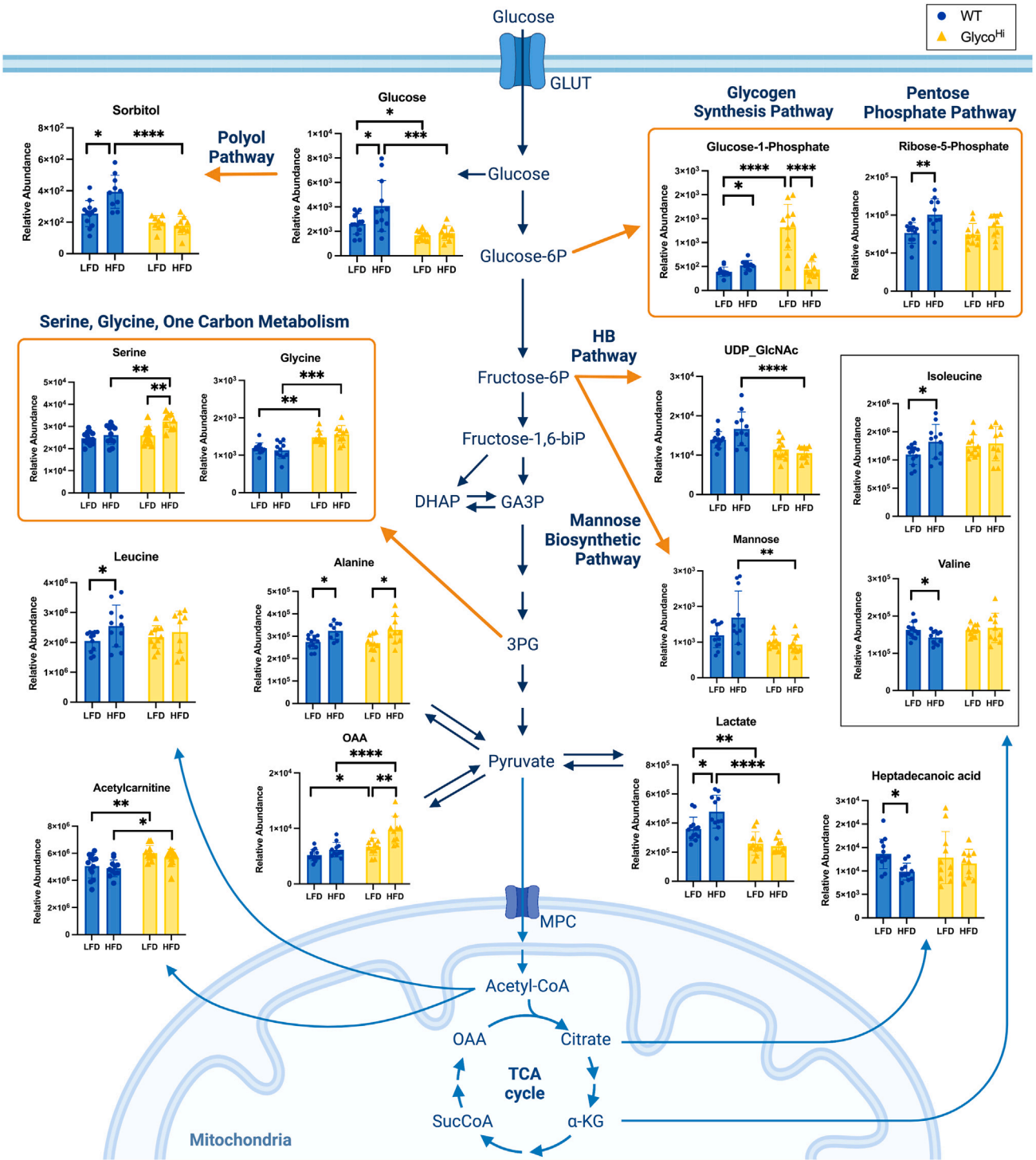

Figure 5. Metabolic profiling reveals fewer HFD-induced changes in Glyco^{Hi} hearts

Male and female WT and Glyco^{Hi} were fed a 16–week low-fat diet (LFD) or high-fat diet (HFD). Metabolites were measured in cardiac tissue by LC/MS. Glycolysis pathways shown with orange arrows indicate metabolites involved in glycolysis ancillary pathways. Data points represent individual biological replicates of combined male and female data (Male: WT/LFD n = 7, WT/HFD n = 8; Glyco^{Hi} n = 5 per group) (Female: WT/LFD n = 5, WT/HFD n = 6; Glyco^{Hi}/LFD = 6, Glyco^{Hi}/HFD = 5). Scatterplot data are represented as the mean ± SD. *p < 0.05, **p < 0.01, ***p < 0.001, ****p < 0.0001 by two-way ANOVA with Tukey multiple comparisons test or unpaired two-tailed Student's *t* test (isoleucine, leucine, and valine). HB = Hexosamine Biosynthetic Pathway, OAA = Oxaloacetate, GLUT = Glucose Transporter, MPC = Mitochondrial Pyruvate Carrier. See also Figure S5.

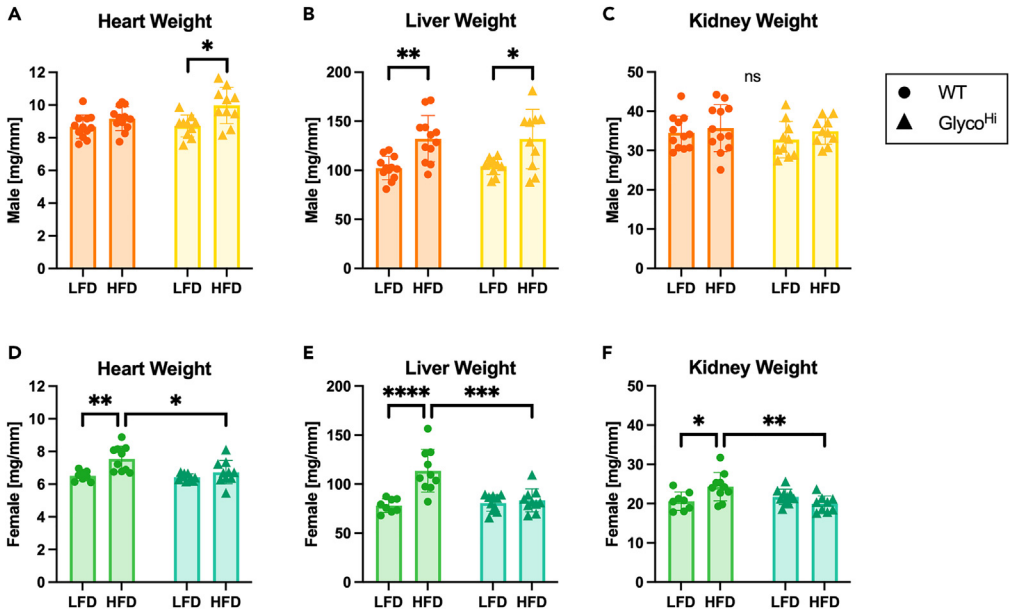

Figure 6. Genotype and sex-dependent alterations in tissue weights in response to HFD

Male and female WT and Glyco^{Hi} were fed a 16-week low-fat diet (LFD) or high-fat diet (HFD).

(A–C) Male tissue weight of hearts (A; This data is the same as in Figure 2D, represented here for ease of comparison to other tissues), livers (B), and kidneys (C) normalized to tibia length (mg/mm) (WT n = 12 per group; Glyco^{Hi} n = 10 per group).

(D–F) Female tissue weight of hearts (D), livers (E), and kidneys (F) normalized to tibia length (mg/mm) (WT/LFD n = 8, WT/HFD n = 10; Glyco^{Hi} n = 10 per group). Scatterplot data are represented as the mean ± SD. *p < 0.05, **p < 0.01, ***p < 0.001 ****p < 0.0001 by two-way ANOVA with Tukey multiple comparisons test. Data points represent individual biological replicates.

increase of PFK-2 activity in Glyco^{Hi} mice. A genotype effect and a strong diet effect were identified by two-way ANOVA analysis of male heart weights. Glyco^{Hi} hearts displayed a slight HFD-induced increase compared to WT (Figure 6A). In contrast, female heart weight increased in WT in response to HFD and did not change in Glyco^{Hi}, with a genotype, diet, and interaction effect identified by two-way ANOVA analysis (Figure 6D). In males, liver weight increased in both WT and Glyco^{Hi} HFD groups while only female WT/HFD displayed an increase in weight (Figures 6B and 6E). Lastly, only the female WT/HFD group had increased kidney weight (Figures 6C and 6F).

We next examined whether the genotype and sex-specific alterations in tissue weights were accompanied by differences in lipid or glycogen accumulation. Both of these energy-storage molecules are affected in obesity and metabolic disorders.[3,9] In the heart, glycogen levels were not responsible for the increase in heart mass, as levels were reduced in both male and female Glyco^{Hi} hearts, irrespective of diet, compared to WT hearts (Figures 7A–7C). Cardiac triglyceride levels also did not correlate with the observed changes in heart weight. Triglyceride levels had a diet-dependent increase only in WT hearts (Figures S6A–S6C). Interestingly, when sexes were combined Glyco^{Hi}/LFD had higher levels of triglycerides compared to WT/LFD. However, Glyco^{Hi} heart triglyceride levels were unresponsive to further increases by HFD. Hepatic triglyceride levels increased in an HFD-dependent manner in WT and to a lesser extent in Glyco^{Hi} males (Figure 7D). Strikingly, only female WT livers had an HFD increase in triglycerides. Glyco^{Hi}/LFD were slightly elevated compared to WT/LFD, but Glyco^{Hi}/LFD and Glyco^{Hi}/HFD had comparable triglyceride levels (Figure 7E). When sexes were combined, Glyco^{Hi} livers had overall lower amounts of triglycerides on an HFD, compared to WT (Figure 7F). Lastly, hepatic glycogen levels were decreased in both WT and Glyco^{Hi} groups in response to HFD. However, WT livers had a more pronounced glycogen decrease as compared to Glyco^{Hi} livers (Figures S6D–S6F).

Subsequently, to examine the divergences in cardiac and liver nutrient accumulation, circulating levels of glucose and insulin were analyzed. Blood glucose levels were elevated in male WT and Glyco^{Hi} HFD groups, yet glucose levels increased only in female WT/HFD (Figures 7G and 7H). Male insulin levels

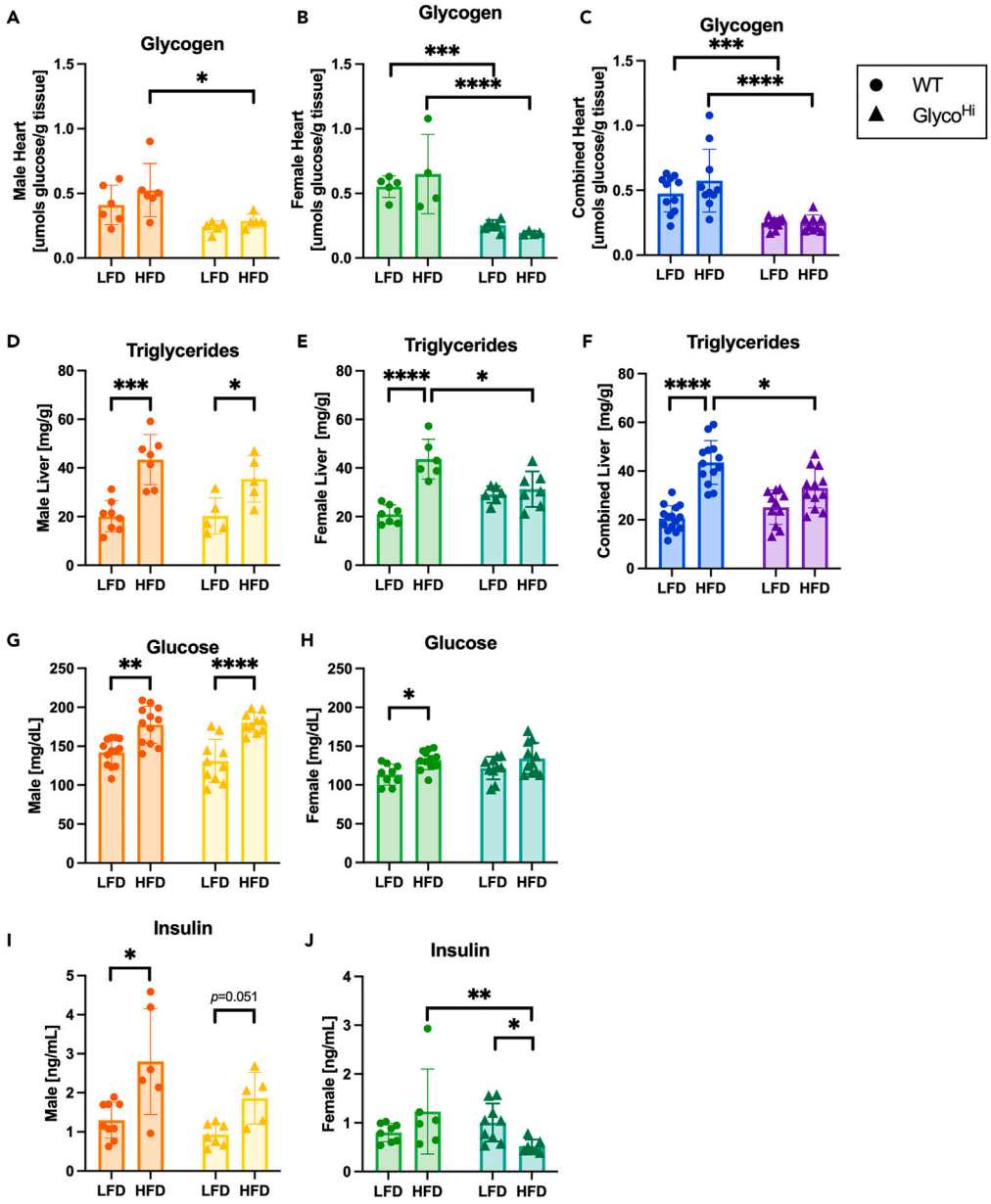

Figure 7. Whole-body metabolism varies between WT and Glyco^{Hi} mice

Cardiac and hepatic tissue from male and female WT and Glyco^{Hi} mice were analyzed for glycogen and triglyceride levels, respectively. Blood glucose and serum insulin levels were measured at the 16-week endpoint in non-fasted mice.

(A) Glycogen content of male hearts (WT n = 6 per group; Glyco^{Hi} n = 5 per group).

(B) Glycogen content of female hearts (WT/LFD n = 5, WT/HFD n = 4; Glyco^{Hi}/LFD n = 6, Glyco^{Hi}/HFD n = 4).

(C) Combined cardiac glycogen content.

(D) Triglyceride content of male livers (WT/LFD n = 8, WT/HFD n = 7; Glyco^{Hi} n = 5 per group).

(E) Triglyceride content of female livers (WT/LFD n = 7, WT/HFD n = 6; Glyco^{Hi}/LFD n = 6, Glyco^{Hi}/HFD n = 7).

(F) Combined liver triglyceride content.

(G) Male blood glucose levels (WT/LFD n = 13, WT/HFD n = 10; Glyco^{Hi} n = 10 per group).

(H) Female blood glucose levels (WT/LFD n = 9, WT/HFD n = 12; Glyco^{Hi}/LFD n = 10, Glyco^{Hi}/HFD n = 11).

(I) Male serum insulin levels (WT/LFD n = 9, WT/HFD n = 6; Glyco^{Hi}/LFD n = 7, Glyco^{Hi}/HFD n = 5).

(J) Female serum insulin levels (WT/LFD n = 8, WT/HFD n = 6; Glyco^{Hi}/LFD n = 9, Glyco^{Hi}/HFD n = 7). Scatterplot data are represented as the mean ± SD. *p < 0.05, **p < 0.01, ***p < 0.001, ****p < 0.0001 by two-way ANOVA with Tukey multiple comparisons test. Data points represent individual biological replicates. See also Figure S6.

mirrored the HFD-induced increase observed in blood glucose with a slightly tempered increase in Glyco^{Hi} males (Figure 7I). Interestingly, female Glyco^{Hi} insulin levels decreased in response to an HFD and had overall reduced insulin levels compared to WT/HFD (Figure 7J). Together, these results signify a greater role of cardiac metabolism in glucose and insulin homeostasis with unique outcomes for liver steatosis and cardiac glycogen storage.

DISCUSSION

We report that after 16 weeks of HFD feeding, increased PFK-2 in Glyco^{Hi} hearts preserved diastolic function. This effect was mediated in part by greater levels of glucose oxidation in Glyco^{Hi}/HFD hearts that had increased PDH activity via decreased PDH phosphorylation (inhibition). Proteomic analysis revealed abated HFD-induced alterations such as lower levels of proteins involved in lipotoxicity and oxidative stress. Additionally, Glyco^{Hi} hearts had a diminished buildup of toxic glucose metabolite intermediates. Lastly, key findings showed increased PFK-2 facilitated positive systemic effects such as lower nutrient accumulation in hepatic tissue and lower incidence of hyperinsulinemia.

Glyco^{Hi} hearts exhibited distinctive adaptations in mitochondrial function. Remarkably, Glyco^{Hi} mitochondria had higher pyruvate-supported respiration and PDH activity, and preserved RCR ratios under long-term HFD conditions compared to WT (Figure 2; Table S2). The most striking confirmation that Glyco^{Hi} mitochondria differed in their response to an HFD was seen in glutamate-supported respiration (Figures 2D–2F). Maximal glutamate-supported respiration and RCRs were significantly decreased in the WT/HFD groups (Table S2). In contrast, these parameters were identical between Glyco^{Hi} LFD and HFD groups. Thus, an unanticipated consequence of enhancing PFK-2 activity is that glutamate-supported respiration is protected from the deleterious effects of HFD. Cumulatively, these data indicate that chronic HFD causes distinct changes in nutrient utilization between WT and Glyco^{Hi} mitochondria.

Cluster and pathway analyses of quantitative proteomics data allowed us to visualize global adaptations that occurred in cardiac metabolism beyond mitochondrial function. Glyco^{Hi} mice showed an overall reduction in proteins involved in the main glycolysis and ancillary glucose pathways. Additionally, Glyco^{Hi} hearts displayed an abated increase in FAO proteins in response to HFD (Figures 4, S9, and S10). Inspection of individual proteins revealed a lower abundance of key fatty acid transport proteins (CD36 and Fabp3) and FAO proteins (i.e., Acca2, Echs1, Eci1, Eci2, and Hadh) in Glyco^{Hi} hearts, compared to WT (Figures S9 and S10). Moreover, proteins involved in antioxidant defense against HFD-induced oxidative stress (Gstm1, Sod2, Txn1, Prdx3, and Prdx5) were also lower in Glyco^{Hi} groups compared to WT (Figures 4 and S4). These differences suggest an attenuated activation of antioxidant defenses, possibly in response to a reduction of lipotoxicity in Glyco^{Hi} hearts. Metabolomic profiles of cardiac tissue further supported this notion. We found that more metabolites were significantly altered in WT hearts compared to Glyco^{Hi} in response to HFD (Figures 5 and S5). Increases in metabolites associated with pathological cardiac remodeling (i.e., sorbitol, R5P, and UDP-GlcNAc) and/or incidence of T2D (i.e., glucose, mannose, and lactate) were attenuated in Glyco^{Hi} compared to WT (Figure 5).[6,29,36] These results concur with proteomic results and are suggestive of a diminished impact of surfeit nutrients in Glyco^{Hi} hearts.

Proteomic and metabolic profiling also revealed other potential protective benefits in Glyco^{Hi} hearts. Protein kinase A (PKA; Prkaca) levels were increased in the female WT/HFD group and had overall reduced expression in both male and female Glyco^{Hi} groups (Figures S14 and S16). PKA activity is increased via β-adrenergic activation in response to sympathetic stimulation. Sympathetic tone is increased in obesity and we have previously reported aberrant PKA activity in the diabetic heart.[37–39] Thus, the lower PKA abundance and resistance to HFD-mediated changes in its content in Glyco^{Hi} hearts further indicate a muted stress response. Moreover, serine and glycine levels were higher in Glyco^{Hi} hearts, in a genotype and diet-dependent manner (Figure 5). Recent studies have reported decreased serine levels in T2D hearts, and conversely, there is a potential for cardioprotective effects of increased serine.[36] Serine, a precursor to glycine, is required for the synthesis of various metabolic intermediates through the serine biosynthetic pathway, another glucose-ancillary pathway. Our finding is particularly intriguing given that although studies report a potential benefit, the role of serine biosynthesis in cardiac disease remains unclear.[36,40]

Despite these positive metabolic effects, not all Glyco^{Hi} changes were interpreted as protective. For example, several proteins associated with improved glucose metabolism had decreased expression in

Glyco^{Hi}/HFD hearts (Glut4 (Scl2a4), Ckm, Got2, and Idh2) (Figures S7, S8, S13, and S15). Additionally, there were modestly elevated acylcarnitine levels which are reported to occur in obesity (Figure 5).[8,41,42] Finally, there were higher levels of glucose-1-phosphate (glycogen synthesis pathway) in Glyco^{Hi}/LFD hearts, relative to WT, despite glycogen levels being overall lower in Glyco^{Hi} hearts (Figures 5 and 7C). Nevertheless, most metabolic changes indicated a tempered adaptation to HFD in Glyco^{Hi} hearts.

Our current findings differed greatly from what we previously found with a short-term metabolic challenge. With 1-week HFD treatment, HFD-dependent changes to mitochondrial respiration were not significantly different between WT and Glyco^{Hi} groups.[20] Notably, PDH activity and regulation differ between the studies. In the previous study, PDK4 levels were 2-fold higher in Glyco^{Hi}/HFD compared to WT/HFD. In the current study, PDK4 levels were similar between HFD-treated groups, and Lon protease was uniquely increased in Glyco^{Hi}/HFD. This temporal change suggests Glyco^{Hi} hearts adapt to overcome PDK4 inhibition of PDH activity. Proteomic and metabolomic analyses are also drastically different when comparing short- and long-term adaptations to HFD. Intriguingly, pathway analysis at 16 weeks revealed a generally opposite effect in both WT and Glyco^{Hi} groups to those seen in 1 week. In our 1-week study, glucose metabolism pathway proteins were decreased in WT, but not Glyco^{Hi}, hearts, whereas FAO proteins were equivalently elevated in both groups.[20] In this study, WT had an increase in proteins involved in glycolysis and FAO, whereas Glyco^{Hi} had a reduction of protein expression in glycolysis and an attenuated increase in FAO (relative to WT/HFD). Furthermore, in this study, increased accumulation of metabolites involved in ancillary glycolysis pathways was only seen in WT/HFD groups which could be in part mediated by the higher expression of early glycolytic proteins. Lastly, a noteworthy difference we found between short and long-term HFD studies was in BCAAs, which are of interest due to their role in diseases such as DCM and their high bioactivity.[43,44] Previously, a buildup of BCAAs was seen only in Glyco^{Hi} hearts after 1 week on HFD. In contrast, after 16 weeks on HFD, WT hearts were the only group to see an HFD-induced change in abundance. The changes identified after a prolonged metabolic challenge highlight a unique adaptive capability of Glyco^{Hi} hearts and the importance of investigating temporal adaptations in metabolic syndrome.

It has been reported that the detrimental effects of high levels of fatty acids in pathological cardiac hypertrophy and heart failure are primarily due to a decrease in glucose oxidation not glycolysis.[45] Lopaschuk et al. found that increasing glucose oxidation, despite a concurrent decrease in glycolysis, was functionally beneficial to the ischemic heart.[45] In our current findings, we also observed a decrease in glycolysis proteins with a concurrent increase in glucose oxidation and preserved function in Glyco^{Hi}/HFD hearts. Moreover, targeting CD36 through pharmacological inhibition or gene expression knockdown has also shown improvements to cardiac health. In a study using transgenic mice with cardiac-specific overexpression of the transcription factor peroxisome proliferator-activated receptor α (PPARα) crossed with CD36 deficient mice, the PPARα transgenic hearts had a complete rescue of their lipotoxic cardiomyopathy phenotype.[26] This improvement was attributed to an increase in myocardial glucose uptake and oxidation, rather than any meaningful changes in fatty acid utilization.

The importance of pyruvate oxidation for both physiological and pathological stress adaptations was recently reported in a mouse model of cardiac-specific deletion of the mitochondrial pyruvate carrier MPC1.[46] In that study, Abel et al. found that MPC1-knockout hearts developed pathological hypertrophy and dilated cardiomyopathy. Collectively, the key results in our study add support to the notion that increasing cardiac glycolysis and glucose oxidation may be beneficial in mitigating HFD-induced changes to proteomic and metabolomic phenotypes.

While we have focused on increased PFK-2 as a means of improving the heart's capacity for glucose oxidation under HFD conditions, previous studies have explored modulating the activity of other points in glucose metabolism as potential interventions. Increasing PDH activity by treatment with dichloroacetate (DCA), a nonspecific PDK inhibitor, is one potential way of increasing glucose oxidation and mitigating diabetic cardiomyopathy.[47,48] Although this treatment has shown promise, DCA treatment is limited by toxicity. In contrast, it is less clear whether strategies that target increased transport of glucose into the heart are sufficient to mitigate diabetic cardiomyopathy. In an early study using *db/db* mice, a T2D and obesity model, the whole-body expression of a GLUT4 transgene improved cardiac contractility and normalized cardiac glucose and palmitate metabolism.[49] However, such beneficial effects may arise from systemic metabolic improvements, as the cardiac-specific expression of

glucose transporters has shown negative outcomes. For example, a study by the Tian group using cardiac-specific GLUT1 transgenic mice revealed that insulin-independent glucose uptake promoted oxidative stress and contractile dysfunction after 20-week HFD.[50] Unlike Glyco^{Hi} mice, GLUT1 transgenic mice had the inability to upregulate myocardial fatty-acid oxidation in response to long-term dietary stress. Likewise, a recent study showed that cardiac-specific transgenic expression of GLUT4 in type 1 diabetic model (T1D) worsened cardiac pathology.[51] This suggests that with hyperglycemia caused by uncontrolled diabetes in T1D, increasing glucose uptake may exacerbate pathology. This could be due to excess glucose shunted into ancillary pathways, which was indicated by cardiac GLUT4 over-expressing hearts having 2.6 times the amount of glycogen as control mice.[51] GLUT1 over-expressing mice also had a significant increase in glycogen (3-fold over WT) on normal chow, ableit glycogen did not increase further after HFD treatment.[50] In contrast, Glyco^{Hi} mice have less glycogen than control mice, a result previously reported by us and others.[18,19,52] These findings highlight the importance and need for studies focused on elucidating and differentiating the mechanisms and effects of diabetic cardiomyopathy in T1D versus T2D.

This work also uncovered an important and unanticipated aspect of Glyco^{Hi} mice regarding whole-body metabolism. Compared to wild type, female Glyco^{Hi} mice, and to a lesser extent male Glyco^{Hi} mice, have improved whole-body glucose homeostasis and diminished nutrient accrual in cardiac and hepatic tissue in response to HFD. This was despite a similar gain in body weight in wild type and Glyco^{Hi} mice. In hepatocytes activation of glycogen synthesis is a principal effect of insulin signaling and as such liver glycogen has an integral role in blood glucose homeostasis.[53] Indeed, it has been reported that lipid-induced insulin resistance in the liver results in a reduction of hepatic glycogen synthesis.[54] Intriguingly, we found that Glyco^{Hi} mice had dampened HFD-induced changes to hepatic lipid and glycogen levels. Our results support that in Glyco^{Hi} mice improved hepatic lipid and glycogen content are indicative of improved glucose homeostasis. Sexual dimorphic differences in mitochondrial function in response to HFD were also apparent in Glyco^{Hi} mice (Figure 2, Table S2). The sex-specific effects are potentially due to the well-known effects of estrogen on both systemic and cardiac metabolism. Indeed, estrogen has the potential to regulate both glucose and fatty acid metabolism.[55,56] Future studies will pursue this possibility using ovariectomized females.

Our findings underscore a previously unexplored capability of cardiac glycolytic activity to influence whole-body metabolism. The connection between cardiac activity and whole-body metabolism is not well understood but could prove critical in understanding physiological and pathological metabolic adaptations. The Olson lab previously reported that cardiac MED13 expression levels can alter systemic energy homeostasis.[57] MED13 is a part of a transcription activator called the mediator complex, and cardiac overexpression resulted in resistance to HFD-induced obesity and enhanced systemic insulin sensitivity, however, the mechanism of action was not identified.[58] Similarly, studies have found that the cardiomyocyte-specific overexpression and knockout of the G-protein coupled receptor kinase 2 and overexpression of the calcium pump SERCA1a, had altered adipose metabolism and beneficial effects to diabetes-induced hyperglycemia, respectively.[59,60] The underlying mechanism of these systemic effects observed here will be the subject of future studies. Some clues are provided by our proteomics data, though. For example, 3-Hydroxy-3-methylglutaryl-CoA lyase (Hmgcl) is a key enzyme in ketogenesis that produces acetoacetate, a biomarker of T2D and insulin resistance.[61] We found Hmgcl levels were lower in female Glyco^{Hi}/HFD compared to WT/HFD and unchanged in male groups, a possible indication of the systemic changes seen in female Glyco^{Hi} mice. These initial studies provide a precedence of heart endocrine factors having beneficial systemic effects on diabetes.

In this study, our findings demonstrate that sustained cardiac glycolysis promotes favorable adaptations during a long-term HFD metabolic challenge. Specifically, increasing glucose oxidation via PFK-2 activity attenuates the cardiac response to nutrient stress. These results underscore the need for therapeutic interventions that normalize nutrient utilization in cardiometabolic diseases. Our work also supports an understudied avenue of research in understanding how cardiac glycolysis mediates systemic effects on glucose tolerance. Future studies will need to identify the underlining mechanisms of how increased PFK-2/PFK-1 mediates the beneficial effects seen in mitochondrial and cardiac function. Additionally, future studies will need to ascertain the relationship between cardiac glucose metabolism and whole-body glucose/insulin homeostasis.

Limitations of the study

There are several limitations of the current study. The phosphatase-deficient PFK-2 transgene is constitutively active from birth. It is thus difficult to separate long-term adaptive genotype effects from dietary effects. The future development of an inducible PFK-2 transgene could overcome this limitation. An inducible transgene could also overcome the mild cardiac hypertrophy that develops in Glyco^{Hi} mice. Indeed, the Hill group previously reported that Glyco^{Hi} mice have hypertrophy accompanied by a mild decrease in ejection.[52] We did not observe a decline in systolic function between Glyco^{Hi} and WT mice in this study. The discrepancy could be due to differences in the age of the mice. It is possible that by 9–11 months, the age used in this study, the differences between genotypes are minimized.

Other limitations include that conclusions made from metabolomics data and pathway analyses are from steady-state observations, and thus do not provide details regarding flux. Due to the unexpected systemic effects of cardiac PFK-2, a limitation of this study is that a complete analysis of physiological measurements was not performed. Future studies will focus on evaluating circulating serum factors, performing glucose tolerance tests, and determining energy expenditure by metabolic cage analysis. An additional limitation is that due to the nature of the mouse physiology, animals do not develop severe T2D in response to HFD. However, mice on 16-week HFD do develop metabolic dysfunction which is akin to the early stages of prediabetes. Because metabolic syndrome is reversible at this stage, our findings provide important insights for potential therapeutic interventions.

STAR★METHODS

Detailed methods are provided in the online version of this paper and include the following:

- KEY RESOURCES TABLE
- RESOURCE AVAILABILITY
  - Lead contact
  - Materials availability
  - Data and code availability
- EXPERIMENTAL MODEL AND STUDY PARTICIPANT DETAILS
  - Rodent housing specifications
  - Rodent age justification
- METHOD DETAILS
  - Echocardiology and QMR analysis
  - Blood and serum measurements
  - Isolation of Cardiac Mitochondria
  - Mitochondrial respiration measurements
  - PDH activity assay
  - NADH oxidase/complex I activity assay
  - CPT1 activity assay
  - Cardiac glycogen and protein carbonyl assay
  - Hepatic triglyceride assay
  - Proteomic analysis
  - Metabolomic analysis
  - Western blot analysis
  - Figure design
- QUANTIFICATION AND STATISTICAL ANALYSIS
  - Statistical details for -omics datasets

SUPPLEMENTAL INFORMATION

Supplemental information can be found online at https://doi.org/10.1016/j.isci.2023.107131.

ACKNOWLEDGMENTS

This work was supported by National Institutes of Health Grants R01HL160955 (to K. M. H.), P30AG050911 (to M. K.), P20GM103447 (to M. K.), R24GM137786 (to M.K.); and by National Science Foundation Graduate

Research Fellowship Program Grant 1849507 (to M. F. M. G.). The content is solely the responsibility of the authors and does not necessarily represent the official views of the National Institutes of Health.

AUTHOR CONTRIBUTIONS

M.F.M.G.: Conceptualization, formal analysis, investigation, project administration, writing- original draft preparation, reviewing, and editing. **S.M.**: Validation, formal analysis, and investigation. A.B.: Visualization, formal analysis, writing-reviewing and editing. **R.N.**: Formal analysis, visualization, and investigation. **C.K.**: Investigation, and formal analysis. **Y.J.**: Investigation, and formal analysis. **S.N.M.**: Investigation, and formal analysis. **M.B.S.**: Resources. **H.G.**: Methodology, validation, formal analysis, investigation, writing-reviewing and editing. **Y.A.C.**: Formal analysis, investigation, writing-reviewing and editing. **M.K.**: Methodology, validation, formal analysis, and investigation, writing-reviewing and editing. **K.H.**: Supervision, funding acquisition, conceptualization, resources, riting- original draft preparation, reviewing and editing.

DECLARATION OF INTERESTS

The authors declare no competing interests.

INCLUSION AND DIVERSITY

We support inclusive, diverse, and equitable conduct of research. One or more of the authors of this paper self-identifies as an underrepresented ethnic minority in their field of research or within their geographical location. One or more of the authors of this paper self-identifies as a gender minority in their field of research. One or more of the authors of this paper self-identifies as living with a disability. One or more of the authors of this paper received support from a program designed to increase minority representation in their field of research. We avoided "helicopter science" practices by including the participating local contributors from the region where we conducted the research as authors on the paper.

Received: November 2, 2022
Revised: April 27, 2023
Accepted: June 10, 2023
Published: June 15, 2023

REFERENCES

1. Haas, A.V., and McDonnell, M.E. (2018). Pathogenesis of Cardiovascular Disease in Diabetes. Endocrinol Metab. Clin. N. Am. *47*, 51–63. https://doi.org/10.1016/j.ecl.2017.10.010.

2. Cosentino, F., Grant, P.J., Aboyans, V., Bailey, C.J., Ceriello, A., Delgado, V., Federici, M., Filippatos, G., Grobbee, D.E., Hansen, T.B., et al. (2020). 2019 ESC Guidelines on diabetes, pre-diabetes, and cardiovascular diseases developed in collaboration with the EASD: The Task Force for diabetes, pre-diabetes, and cardiovascular diseases of the European Society of Cardiology (ESC) and the European Association for the Study of Diabetes (EASD). Eur. Heart J. *41*, 255–323. https://doi.org/10.1093/eurheartj/ehz486.

3. Bozkurt, B., Aguilar, D., Deswal, A., Dunbar, S.B., Francis, G.S., Horwich, T., Jessup, M., Kosiborod, M., Pritchett, A.M., Ramasubbu, K., et al. (2016). Contributory Risk and Management of Comorbidities of Hypertension, Obesity, Diabetes Mellitus, Hyperlipidemia, and Metabolic Syndrome in Chronic Heart Failure: A Scientific Statement From the American Heart Association. Circulation *134*, e535–e578. https://doi.org/10.1161/CIR.0000000000000450.

4. Nakamura, M., and Sadoshima, J. (2020). Cardiomyopathy in obesity, insulin resistance and diabetes. J. Physiol. *598*, 2977–2993. https://doi.org/10.1113/JP276747.

5. Depre, C., Vanoverschelde, J.L., and Taegtmeyer, H. (1999). Glucose for the heart. Circulation *99*, 578–588. https://doi.org/10.1161/01.cir.99.4.578.

6. Gibb, A.A., and Hill, B.G. (2018). Metabolic Coordination of Physiological and Pathological Cardiac Remodeling. Circ. Res. *123*, 107–128. https://doi.org/10.1161/CIRCRESAHA.118.312017.

7. Randle, P.J., Garland, P.B., Hales, C.N., and Newsholme, E.A. (1963). The glucose fatty-acid cycle. Its role in insulin sensitivity and the metabolic disturbances of diabetes mellitus. Lancet *1*, 785–789. https://doi.org/10.1016/s0140-6736(63)91500-9.

8. Stanley, W.C., Lopaschuk, G.D., and McCormack, J.G. (1997). Regulation of energy substrate metabolism in the diabetic heart. Cardiovasc. Res. *34*, 25–33. https://doi.org/10.1016/s0008-6363(97)00047-3.

9. Bugger, H., and Abel, E.D. (2014). Molecular mechanisms of diabetic cardiomyopathy. Diabetologia *57*, 660–671. https://doi.org/10.1007/s00125-014-3171-6.

10. Okar, D.A., Manzano, A., Navarro-Sabatè, A., Riera, L., Bartrons, R., and Lange, A.J. (2001). PFK-2/FBPase-2: maker and breaker of the essential biofactor fructose-2,6-bisphosphate. Trends Biochem. Sci. *26*, 30–35.

11. Hue, L., and Rider, M.H. (1987). Role of fructose 2,6-bisphosphate in the control of glycolysis in mammalian tissues. Biochem. J. *245*, 313–324.

12. Marsin, A.S., Bertrand, L., Rider, M.H., Deprez, J., Beauloye, C., Vincent, M.F., Van den Berghe, G., Carling, D., and Hue, L. (2000). Phosphorylation and activation of heart PFK-2 by AMPK has a role in the stimulation of glycolysis during ischaemia. Curr. Biol. *10*, 1247–1255.

13. Depré, C., Rider, M.H., and Hue, L. (1998). Mechanisms of control of heart glycolysis. Eur. J. Biochem. *258*, 277–290. https://doi.org/10.1046/j.1432-1327.1998.2580277.x.

14. Bockus, L.B., Matsuzaki, S., Vadvalkar, S.S., Young, Z.T., Giorgione, J.R., Newhardt, M.F., Kinter, M., and Humphries, K.M. (2017). Cardiac Insulin Signaling Regulates

Glycolysis Through Phosphofructokinase 2 Content and Activity. J. Am. Heart Assoc. *6*, e007159. https://doi.org/10.1161/JAHA.117.007159.

15. Bowker-Kinley, M.M., Davis, W.I., Wu, P., Harris, R.A., and Popov, K.M. (1998). Evidence for existence of tissue-specific regulation of the mammalian pyruvate dehydrogenase complex. Biochem. J. *329*, 191–196. https://doi.org/10.1042/bj3290191.

16. Rardin, M.J., Wiley, S.E., Naviaux, R.K., Murphy, A.N., and Dixon, J.E. (2009). Monitoring phosphorylation of the pyruvate dehydrogenase complex. Anal. Biochem. *389*, 157–164. https://doi.org/10.1016/j.ab.2009.03.040.

17. Sugden, M.C., and Holness, M.J. (2006). Mechanisms underlying regulation of the expression and activities of the mammalian pyruvate dehydrogenase kinases. Arch. Physiol. Biochem. *112*, 139–149. https://doi.org/10.1080/13813450600935263.

18. Wang, Q., Donthi, R.V., Wang, J., Lange, A.J., Watson, L.J., Jones, S.P., and Epstein, P.N. (2008). Cardiac phosphatase-deficient 6-phosphofructo-2-kinase/fructose-2,6-bisphosphatase increases glycolysis, hypertrophy, and myocyte resistance to hypoxia. Am. J. Physiol. Heart Circ. Physiol. *294*, H2889–H2897. https://doi.org/10.1152/ajpheart.91501.2007.

19. Batushansky, A., Matsuzaki, S., Newhardt, M.F., West, M.S., Griffin, T.M., and Humphries, K.M. (2019). GC-MS metabolic profiling reveals fructose-2,6-bisphosphate regulates branched chain amino acid metabolism in the heart during fasting. Metabolomics *15*, 18. https://doi.org/10.1007/s11306-019-1478-5.

20. Newhardt, M.F., Batushansky, A., Matsuzaki, S., Young, Z.T., West, M., Chin, N.C., Szweda, L.I., Kinter, M., and Humphries, K.M. (2019). Enhancing cardiac glycolysis causes an increase in PDK4 content in response to short-term high-fat diet. J. Biol. Chem. *294*, 16831–16845. https://doi.org/10.1074/jbc.RA119.010371.

21. Riehle, C., and Bauersachs, J. (2018). Of mice and men: models and mechanisms of diabetic cardiomyopathy. Basic Res. Cardiol. *114*, 2. https://doi.org/10.1007/s00395-018-0711-0.

22. Chong, C.R., Clarke, K., and Levelt, E. (2017). Metabolic Remodeling in Diabetic Cardiomyopathy. Cardiovasc. Res. *113*, 422–430. https://doi.org/10.1093/cvr/cvx018.

23. Salabei, J.K., Gibb, A.A., and Hill, B.G. (2014). Comprehensive measurement of respiratory activity in permeabilized cells using extracellular flux analysis. Nat. Protoc. *9*, 421–438. https://doi.org/10.1038/nprot.2014.018.

24. Crewe, C., Schafer, C., Lee, I., Kinter, M., and Szweda, L.I. (2017). Regulation of Pyruvate Dehydrogenase Kinase 4 in the Heart through Degradation by the Lon Protease in Response to Mitochondrial Substrate Availability. J. Biol. Chem. *292*, 305–312. https://doi.org/10.1074/jbc.M116.754127.

25. Lopaschuk, G.D., Ussher, J.R., Folmes, C.D.L., Jaswal, J.S., and Stanley, W.C. (2010). Myocardial fatty acid metabolism in health and disease. Physiol. Rev. *90*, 207–258. https://doi.org/10.1152/physrev.00015.2009.

26. Yang, J., Sambandam, N., Han, X., Gross, R.W., Courtois, M., Kovacs, A., Febbraio, M., Finck, B.N., and Kelly, D.P. (2007). CD36 deficiency rescues lipotoxic cardiomyopathy. Circ. Res. *100*, 1208–1217. https://doi.org/10.1161/01.RES.0000264104.25265.b6.

27. Furuhashi, M. (2019). Fatty Acid-Binding Protein 4 in Cardiovascular and Metabolic Diseases. J. Atherosclerosis Thromb. *26*, 216–232. https://doi.org/10.5551/jat.48710.

28. Abel, E.D. (2021). Insulin signaling in the heart. Am. J. Physiol. Endocrinol. Metab. *321*, E130–E145. https://doi.org/10.1152/ajpendo.00158.2021.

29. Kolwicz, S.C., Jr., Purohit, S., and Tian, R. (2013). Cardiac metabolism and its interactions with contraction, growth, and survival of cardiomyocytes. Circ. Res. *113*, 603–616. https://doi.org/10.1161/CIRCRESAHA.113.302095.

30. Shah, M.S., and Brownlee, M. (2016). Molecular and Cellular Mechanisms of Cardiovascular Disorders in Diabetes. Circ. Res. *118*, 1808–1829. https://doi.org/10.1161/CIRCRESAHA.116.306923.

31. Menni, C., Fauman, E., Erte, I., Perry, J.R.B., Kastenmüller, G., Shin, S.Y., Petersen, A.K., Hyde, C., Psatha, M., Ward, K.J., et al. (2013). Biomarkers for type 2 diabetes and impaired fasting glucose using a nontargeted metabolomics approach. Diabetes *62*, 4270–4276. https://doi.org/10.2337/db13-0570.

32. Peddinti, G., Cobb, J., Yengo, L., Froguel, P., Kravić, J., Balkau, B., Tuomi, T., Aittokallio, T., and Groop, L. (2017). Early metabolic markers identify potential targets for the prevention of type 2 diabetes. Diabetologia *60*, 1740–1750. https://doi.org/10.1007/s00125-017-4325-0.

33. Li, D.K., Smith, L.E., Rookyard, A.W., Lingam, S.J., Koay, Y.C., McEwen, H.P., Twigg, S.M., Don, A.S., O'Sullivan, J.F., Cordwell, S.J., and White, M.Y. (2022). Multi-omics of a pre-clinical model of diabetic cardiomyopathy reveals increased fatty acid supply impacts mitochondrial metabolic selectivity. J. Mol. Cell. Cardiol. *164*, 92–109. https://doi.org/10.1016/j.yjmcc.2021.11.009.

34. Neishabouri, S.H., Hutson, S.M., and Davoodi, J. (2015). Chronic activation of mTOR complex 1 by branched chain amino acids and organ hypertrophy. Amino Acids *47*, 1167–1182. https://doi.org/10.1007/s00726-015-1944-y.

35. Kimball, S.R., Shantz, L.M., Horetsky, R.L., and Jefferson, L.S. (1999). Leucine regulates translation of specific mRNAs in L6 myoblasts through mTOR-mediated changes in availability of eIF4E and phosphorylation of ribosomal protein S6. J. Biol. Chem. *274*, 11647–11652. https://doi.org/10.1074/jbc.274.17.11647.

36. Tran, D.H., and Wang, Z.V. (2019). Glucose Metabolism in Cardiac Hypertrophy and Heart Failure. J. Am. Heart Assoc. *8*, e012673. https://doi.org/10.1161/JAHA.119.012673.

37. Lambert, G.W., Straznicky, N.E., Lambert, E.A., Dixon, J.B., and Schlaich, M.P. (2010). Sympathetic nervous activation in obesity and the metabolic syndrome–causes, consequences and therapeutic implications. Pharmacol. Ther. *126*, 159–172. https://doi.org/10.1016/j.pharmthera.2010.02.002.

38. Bockus, L.B., and Humphries, K.M. (2015). cAMP-dependent Protein Kinase (PKA) Signaling Is Impaired in the Diabetic Heart. J. Biol. Chem. *290*, 29250–29258. https://doi.org/10.1074/jbc.M115.681767 S0021-9258(20)39543-0.

39. Eyster, C.A., Matsuzaki, S., Newhardt, M.F., Giorgione, J.R., and Humphries, K.M. (2020). Diabetes induced decreases in PKA signaling in cardiomyocytes: The role of insulin. PLoS One *15*, e0231806. https://doi.org/10.1371/journal.pone.0231806.

40. Padrón-Barthe, L., Villalba-Orero, M., Gómez-Salinero, J.M., Acín-Pérez, R., Cogliati, S., López-Olañeta, M., Ortiz-Sánchez, P., Bonzón-Kulichenko, E., Vázquez, J., García-Pavía, P., et al. (2018). Activation of Serine One-Carbon Metabolism by Calcineurin Abeta1 Reduces Myocardial Hypertrophy and Improves Ventricular Function. J. Am. Coll. Cardiol. *71*, 654–667. https://doi.org/10.1016/j.jacc.2017.11.067.

41. Vileigas, D.F., Harman, V.M., Freire, P.P., Marciano, C.L.C., Sant'Ana, P.G., de Souza, S.L.B., Mota, G.A.F., da Silva, V.L., Campos, D.H.S., Padovani, C.R., et al. (2019). Landscape of heart proteome changes in a diet-induced obesity model. Sci. Rep. *9*, 18050. https://doi.org/10.1038/s41598-019-54522-2.

42. Shao, D., and Tian, R. (2015). Glucose Transporters in Cardiac Metabolism and Hypertrophy. Compr. Physiol. *6*, 331–351. https://doi.org/10.1002/cphy.c150016.

43. Cummings, N.E., Williams, E.M., Kasza, I., Konon, E.N., Schaid, M.D., Schmidt, B.A., Poudel, C., Sherman, D.S., Yu, D., Arriola Apelo, S.I., et al. (2018). Restoration of metabolic health by decreased consumption of branched-chain amino acids. J. Physiol. *596*, 623–645. https://doi.org/10.1113/JP275075.

44. Huang, Y., Zhou, M., Sun, H., and Wang, Y. (2011). Branched-chain amino acid metabolism in heart disease: an epiphenomenon or a real culprit? Cardiovasc. Res. *90*, 220–223. https://doi.org/10.1093/cvr/cvr070.

45. Lopaschuk, G.D., Wambolt, R.B., and Barr, R.L. (1993). An imbalance between glycolysis and glucose oxidation is a possible explanation for the detrimental effects of high levels of fatty acids during aerobic reperfusion of ischemic hearts. J. Pharmacol. Exp. Therapeut. *264*, 135–144.

46. Zhang, Y., Taufalele, P.V., Cochran, J.D., Robillard-Frayne, I., Marx, J.M., Soto, J., Rauckhorst, A.J., Tayyari, F., Pewa, A.D., Gray, L.R., et al. (2020). Mitochondrial pyruvate carriers are required for myocardial stress

adaptation. Nat. Metab. *2*, 1248–1264. https://doi.org/10.1038/s42255-020-00288-1.

47. Nicholl, T.A., Lopaschuk, G.D., and McNeill, J.H. (1991). Effects of free fatty acids and dichloroacetate on isolated working diabetic rat heart. Am. J. Physiol. *261*, H1053–H1059. https://doi.org/10.1152/ajpheart.1991.261.4.H1053.

48. Le Page, L.M., Rider, O.J., Lewis, A.J., Ball, V., Clarke, K., Johansson, E., Carr, C.A., Heather, L.C., and Tyler, D.J. (2015). Increasing Pyruvate Dehydrogenase Flux as a Treatment for Diabetic Cardiomyopathy: A Combined 13C Hyperpolarized Magnetic Resonance and Echocardiography Study. Diabetes *64*, 2735–2743. https://doi.org/10.2337/db14-1560.

49. Belke, D.D., Larsen, T.S., Gibbs, E.M., and Severson, D.L. (2000). Altered metabolism causes cardiac dysfunction in perfused hearts from diabetic (db/db) mice. Am. J. Physiol. Endocrinol. Metab. *279*, E1104–E1113. https://doi.org/10.1152/ajpendo.2000.279.5.E1104.

50. Yan, J., Young, M.E., Cui, L., Lopaschuk, G.D., Liao, R., and Tian, R. (2009). Increased glucose uptake and oxidation in mouse hearts prevent high fatty acid oxidation but cause cardiac dysfunction in diet-induced obesity. Circulation *119*, 2818–2828. https://doi.org/10.1161/CIRCULATIONAHA.108.832915 CIRCULATIONAHA.108.832915.

51. Wende, A.R., Schell, J.C., Ha, C.M., Pepin, M.E., Khalimonchuk, O., Schwertz, H., Pereira, R.O., Brahma, M.K., Tuinei, J., Contreras-Ferrat, A., et al. (2020). Maintaining Myocardial Glucose Utilization in Diabetic Cardiomyopathy Accelerates Mitochondrial Dysfunction. Diabetes *69*, 2094–2111. https://doi.org/10.2337/db19-1057.

52. Gibb, A.A., Epstein, P.N., Uchida, S., Zheng, Y., McNally, L.A., Obal, D., Katragadda, K., Trainor, P., Conklin, D.J., Brittian, K.R., et al. (2017). Exercise-Induced Changes in Glucose Metabolism Promote Physiological Cardiac Growth. Circulation *136*, 2144–2157. https://doi.org/10.1161/CIRCULATIONAHA.117.028274.

53. Petersen, M.C., Vatner, D.F., and Shulman, G.I. (2017). Regulation of hepatic glucose metabolism in health and disease. Nat. Rev. Endocrinol. *13*, 572–587. https://doi.org/10.1038/nrendo.2017.80.

54. Nozaki, Y., Petersen, M.C., Zhang, D., Vatner, D.F., Perry, R.J., Abulizi, A., Haedersdal, S., Zhang, X.M., Butrico, G.M., Samuel, V.T., et al. (2020). Metabolic control analysis of hepatic glycogen synthesis in vivo. Proc. Natl. Acad. Sci. USA *117*, 8166–8176. https://doi.org/10.1073/pnas.1921694117.

55. Wang, T., McDonald, C., Petrenko, N.B., Leblanc, M., Wang, T., Giguere, V., Evans, R.M., Patel, V.V., and Pei, L. (2015). Estrogen-related receptor alpha (ERRalpha) and ERRgamma are essential coordinators of cardiac metabolism and function. Mol. Cell Biol. *35*, 1281–1298. https://doi.org/10.1128/MCB.01156-14.

56. Li, S., and Gupte, A.A. (2017). The Role of Estrogen in Cardiac Metabolism and Diastolic Function. Methodist Debakey Cardiovasc. J. *13*, 4–8. https://doi.org/10.14797/mdcj-13-1-4.

57. Grueter, C.E., van Rooij, E., Johnson, B.A., DeLeon, S.M., Sutherland, L.B., Qi, X., Gautron, L., Elmquist, J.K., Bassel-Duby, R., and Olson, E.N. (2012). A cardiac microRNA governs systemic energy homeostasis by regulation of MED13. Cell *149*, 671–683. https://doi.org/10.1016/j.cell.2012.03.029.

58. Baskin, K.K., Grueter, C.E., Kusminski, C.M., Holland, W.L., Bookout, A.L., Satapati, S., Kong, Y.M., Burgess, S.C., Malloy, C.R., Scherer, P.E., et al. (2014). MED13-dependent signaling from the heart confers leanness by enhancing metabolism in adipose tissue and liver. EMBO Mol. Med. *6*, 1610–1621. https://doi.org/10.15252/emmm.201404218.

59. Woodall, B.P., Gresham, K.S., Woodall, M.A., Valenti, M.C., Cannavo, A., Pfleger, J., Chuprun, J.K., Drosatos, K., and Koch, W.J. (2019). Alteration of myocardial GRK2 produces a global metabolic phenotype. JCI Insight *5*, e123848. https://doi.org/10.1172/jci.insight.123848.

60. Waller, A.P., Kalyanasundaram, A., Hayes, S., Periasamy, M., and Lacombe, V.A. (2015). Sarcoplasmic reticulum Ca2+ ATPase pump is a major regulator of glucose transport in the healthy and diabetic heart. Biochim. Biophys. Acta *1852*, 873–881. https://doi.org/10.1016/j.bbadis.2015.01.009.

61. Chen, Z.Z., and Gerszten, R.E. (2020). Metabolomics and Proteomics in Type 2 Diabetes. Circ. Res. *126*, 1613–1627. https://doi.org/10.1161/CIRCRESAHA.120.315898.

62. Jackson, S.J., Andrews, N., Ball, D., Bellantuono, I., Gray, J., Hachoumi, L., Holmes, A., Latcham, J., Petrie, A., Potter, P., et al. (2017). Does age matter? The impact of rodent age on study outcomes. Lab. Anim. *51*, 160–169. https://doi.org/10.1177/0023677216653984.

63. Vadvalkar, S.S., Matsuzaki, S., Eyster, C.A., Giorgione, J.R., Bockus, L.B., Kinter, C.S., Kinter, M., and Humphries, K.M. (2017). Decreased Mitochondrial Pyruvate Transport Activity in the Diabetic Heart: ROLE OF MITOCHONDRIAL PYRUVATE CARRIER 2 (MPC2) ACETYLATION. J. Biol. Chem. *292*, 4423–4433. https://doi.org/10.1074/jbc.M116.753509 M116.753509.

64. Ushakova, A.V., Grivennikova, V.G., Ohnishi, T., and Vinogradov, A.D. (1999). Triton X-100 as a specific inhibitor of the mammalian NADH-ubiquinone oxidoreductase (Complex I). Biochim. Biophys. Acta *1409*, 143–153. https://doi.org/10.1016/s0005-2728(98)00156-x.

65. Griesel, B.A., Weems, J., Russell, R.A., Abel, E.D., Humphries, K., and Olson, A.L. (2010). Acute inhibition of fatty acid import inhibits GLUT4 transcription in adipose tissue, but not skeletal or cardiac muscle tissue, partly through liver X receptor (LXR) signaling. Diabetes *59*, 800–807. https://doi.org/10.2337/db09-1542.

66. Folch, J., Lees, M., and Sloane Stanley, G.H. (1957). A simple method for the isolation and purification of total lipides from animal tissues. J. Biol. Chem. *226*, 497–509.

67. Mann, S.N., Hadad, N., Nelson Holte, M., Rothman, A.R., Sathiaseelan, R., Ali Mondal, S., Agbaga, M.P., Unnikrishnan, A., Subramaniam, M., Hawse, J., et al. (2020). Health benefits attributed to 17alpha-estradiol, a lifespan-extending compound, are mediated through estrogen receptor alpha. Elife *9*, e59616. https://doi.org/10.7554/eLife.59616.

68. Puente, B.N., Kimura, W., Muralidhar, S.A., Moon, J., Amatruda, J.F., Phelps, K.L., Grinsfelder, D., Rothermel, B.A., Chen, R., Garcia, J.A., et al. (2014). The oxygen-rich postnatal environment induces cardiomyocyte cell-cycle arrest through DNA damage response. Cell *157*, 565–579. https://doi.org/10.1016/j.cell.2014.03.032 S0092-8674(14)00407-3.

69. Nakada, Y., Canseco, D.C., Thet, S., Abdisalaam, S., Asaithamby, A., Santos, C.X., Shah, A.M., Zhang, H., Faber, J.E., Kinter, M.T., et al. (2017). Hypoxia induces heart regeneration in adult mice. Nature *541*, 222–227. https://doi.org/10.1038/nature20173 nature20173.

70. Rindler, P.M., Plafker, S.M., Szweda, L.I., and Kinter, M. (2013). High dietary fat selectively increases catalase expression within cardiac mitochondria. J. Biol. Chem. *288*, 1979–1990. https://doi.org/10.1074/jbc.M112.412890 M112.412890.

71. MacLean, B., Tomazela, D.M., Shulman, N., Chambers, M., Finney, G.L., Frewen, B., Kern, R., Tabb, D.L., Liebler, D.C., and MacCoss, M.J. (2010). Skyline: an open source document editor for creating and analyzing targeted proteomics experiments. Bioinformatics *26*, 966–968. https://doi.org/10.1093/bioinformatics/btq054 btq054.

72. Carroll, P.A., Diolaiti, D., McFerrin, L., Gu, H., Djukovic, D., Du, J., Cheng, P.F., Anderson, S., Ulrich, M., Hurley, J.B., et al. (2015). Deregulated Myc Requires MondoA/Mlx for Metabolic Reprogramming and Tumorigenesis. Cancer Cell *27*, 271–285.

73. Gu, H., Zhang, P., Zhu, J., and Raftery, D. (2015). Globally Optimized Targeted Mass Spectrometry (GOT-MS). Anal. Chem. *87*, 12355–12362.

74. Gu, H., Carroll, P.A., Du, J., Zhu, J., Neto, F.C., Eisenman, R.N., and Raftery, D. (2016). Quantitative Method to Investigate the Balance between Metabolism and Proteome Biomass: Starting from Glycine. Angew. Chem., Int. Ed. Engl. *55*, 15646–15650. https://doi.org/10.1002/anie.201609236.

75. Shi, X., Wang, S., Jasbi, P., Turner, C., Hrovat, J., Wei, Y., Liu, J., and Gu, H. (2019). Database-Assisted Globally Optimized Targeted Mass Spectrometry (dGOT-MS): Broad and Reliable Metabolomics Analysis with Enhanced Identification. Anal. Chem. *91*, 13737–13745. https://doi.org/10.1021/acs.analchem.9b03107.

76. Jasbi, P., Mitchell, N.M., Shi, X., Grys, T.E., Wei, Y., Liu, L., Lake, D.F., and Gu, H. (2019). Coccidioidomycosis Detection Using Targeted Plasma and Urine Metabolic Profiling. J. Proteome Res. *18*, 2791–2802. https://doi.org/10.1021/acs.jproteome.9b00100.

77. Eghlimi, R., Shi, X., Hrovat, J., Xi, B., and Gu, H. (2020). Triple Negative Breast Cancer Detection Using LC-MS/MS Lipidomic Profiling. J. Proteome Res. *19*, 2367–2378. https://doi.org/10.1021/acs.jproteome.0c00038.

78. Jasbi, P., Shi, X., Chu, P., Elliott, N., Hudson, H., Jones, D., Serrano, G., Chow, B., Beach, T.G., Liu, L., et al. (2021). Metabolic Profiling of Neocortical Tissue Discriminates Alzheimer's Disease from Mild Cognitive Impairment, High Pathology Controls, and Normal Controls. J. Proteome Res. *20*, 4303–4317. https://doi.org/10.1021/acs.jproteome.1c00290.

79. Pang, Z., Zhou, G., Ewald, J., Chang, L., Hacariz, O., Basu, N., and Xia, J. (2022). Using MetaboAnalyst 5.0 for LC-HRMS spectra processing, multi-omics integration and covariate adjustment of global metabolomics data. Nat. Protoc. *17*, 1735–1761. https://doi.org/10.1038/s41596-022-00710-w.

80. Szklarczyk, D., Gable, A.L., Lyon, D., Junge, A., Wyder, S., Huerta-Cepas, J., Simonovic, M., Doncheva, N.T., Morris, J.H., Bork, P., et al. (2019). STRING v11: protein-protein association networks with increased coverage, supporting functional discovery in genome-wide experimental datasets. Nucleic Acids Res. *47*, D607–D613. https://doi.org/10.1093/nar/gky1131.

STAR★METHODS

KEY RESOURCES TABLE

REAGENT or RESOURCE	SOURCE	IDENTIFIER
Antibodies		
Pyruvate dehydrogenase (C54G1) Rabbit mAb	Cell Signaling Tech.	Cat#3205S; RRID:AB_2162926
Phospho-pyruvate dehydrogenase (S293) (polyclonal) Rabbit	Cell Signaling Tech.	Cat#31866S; RRID:AB_2799014
Acetyl-CoA carboxylase (C83B10) Rabbit mAb	Cell Signaling Tech.	Cat#3676S; RRID:AB_2219397
Phospho-acetyl-CoA carboxylase (S79) (polyclonal) Rabbit	Cell Signaling Tech.	Cat#3661S; RRID:AB_330337
Akt (pan) (C67E7) Rabbit mAb	Cell Signaling Tech.	Cat#4691S; RRID:AB_915783
Phospho-Akt (S473) (D9E) Rabbit mAb	Cell Signaling Tech.	Cat#4060S; RRID:AB_2315049
4E-BP1 (polyclonal) Rabbit	Cell Signaling Tech.	Cat#9452S; RRID:AB_331692
Phospho-4E-BP1 (T37/46) (236B4) Rabbit mAb	Cell Signaling Tech.	Cat#2855S; RRID:AB_560835
Chemicals, peptides, and recombinant proteins		
Bovine serum albumin	MilliporeSigma	Cat#A88065G
Palmitoyl-DL-carnitine chloride	MilliporeSigma	Cat#P4509
Critical commercial assays		
Insulin Rodent (Mouse/Rat) Chemiluminescence ELISA	ALPCO	Cat#80-INSMR-CH01, CH10
Glycogen Assay Kit	MilliporeSigma	Cat#MAK016-1KT
Protein Carbonyl Content Assay Kit	abcam	Cat#Ab126287
Deposited data		
Proteomics and metabolomics data		https://doi.org/10.5281/zenodo.7946893
Experimental models: Organisms/strains		
FVB/NJ mice (for breeding)	Jackson Laboratory	Cat#001800
Software and algorithms		
GraphPad Prism 9	Dotmatics	www.graphpad.com
Skyline	MacCoss Lab Software	https://skyline.ms/project/home/software/Skyline/begin.view
Other		
Rodent Diet with 10 kcal% Fat (Matching Sucrose to D12492)	Research Diets	Cat#D12450Ji
Rodent Diet with 60 kcal% Fat	Research Diets	Cat#D12492i

RESOURCE AVAILABILITY

Lead contact

Further information and requests for resources should be directed to and will be fulfilled by the Lead contact, Kenneth M. Humphries (Kenneth-Humphries@omrf.org).

Materials availability

This study did not generate new unique reagents.

Data and code availability

- Data: All proteomic and metabolomic raw data has been deposited into Zenodo. DOIs are listed in the key resources table.

- Code: No new code was generated during the course of this study.
- All other Data: Any additional data are available upon request by contacting lead contact, Kenneth M. Humphries (Kenneth-Humphries@omrf.org).

EXPERIMENTAL MODEL AND STUDY PARTICIPANT DETAILS

Female and male littermates of mature adult transgenic Glyco^{Hi} and WT mice on the FVB/NJ background (9–11 months old, at start of treatment) were used in this study. Glyco^{Hi} mice were obtained from the Epstein laboratory at the University of Louisville, and the development of these transgenic mice has previously been described.[18] Briefly, Glyco^{Hi} mice have cardiac-specific expression of a phosphatase-deficient PFK-2 bound to the α-myosin heavy-chain promoter. Mice were randomized to either a low-fat diet (10% fat, 70% carbohydrate, and 20% protein, by kcals) treatment or a high-fat diet (60% fat, 20% carbohydrate, and 20% protein, by kcals; Research Diets) with *ad-lib* access for 16 weeks. Exclusion criteria was defined as animals that did not gain weight on high fat diet (n = 1, Glyco^{Hi} male). Mice were euthanized by cervical dislocation and tissues were collected at 7-8AM without removal of food prior to euthanasia. Animals were not fasted prior to euthanasia due to the need to assess PDH activity, which is significantly affected by fasting conditions. All procedures were approved by the Oklahoma Medical Research Foundation Animal Care and Use Committee.

Rodent housing specifications

Mice were group-housed and maintained on a 14-h light/ dark cycle (light from 06:00 to 20:00). Temperature of mouse holding rooms was kept at 70–74°F.

Rodent age justification

The mouse age range (9–11 months) was used as it is within the equivalent human age-range (37–45 years) of the average onset of metabolic syndrome/type 2 diabetes (Center of Disease Control and Prevention [CDC], 2021). This age-range was chosen following the recommendations for best practice which state that the age of rodents used in a study should be based on the development of the disease being studied.[62] Not only may this practice increase the translation of rodent models to humans, but also allows for the comparison of the experimental results in our first study to the current study as we continue testing our hypotheses. At this age, mice are no longer undergoing developmental changes which minimizes the age differences that would be seen for example between 2 months vs 4 months of age. Nevertheless, to minimize any age-dependent bias in the data, we confirmed that all age-groups were represented across all experiments performed.

METHOD DETAILS

Echocardiology and QMR analysis

Echocardiography was performed on a subset of male mice using a Siemens Acuson CV-70 equipped with a 13MHz probe at baseline and post-treatment timepoints to assess systolic and diastolic function of the mice. Mice were anesthetized by 1% isoflurane. Left Ventricular concentric remodeling was calculated as = (LVpwd/tibia length)/(LVIDD/tibia length).

We performed sample size calculation (using the online Statulator tool) using Ea/Aa data from a previous study to determine that n = 5 is required for echocardiography to achieve a power of 80% and a level of significance of 5%. When using the Ea/Aa data from the current study (pooled SD for Ea/Aa = 0.081), n = 5 is required to detect a 0.15 difference in group means. Thus, the sample size was sufficient to reach statistical significance and demonstrates protection in the Glyco^{Hi} hearts. QMR analysis was performed using the EchoMRI™ system body composition analyzer for live small animals (rats, mice) and organs.

Blood and serum measurements

Serum insulin levels were measured using an insulin ELISA (ALPCO). Blood was collected immediately following euthanasia by cardiac puncture. Blood glucose levels were measured via tail snip using a blood glucose monitor (Bayer Contour) immediately after euthanasia and before tissue collection.

Isolation of Cardiac Mitochondria

Heart mitochondria were isolated by differential centrifugation.[63] Following euthanasia and blood collection, the chest cavity was opened, and the heart was flushed with 5 mL of isolation buffer (Iso buffer) containing 210 mM mannitol, 70 mM sucrose, 5.0 mM MOPS, and 1.0 mM EDTA, pH 7.4, by injection into the left ventricle. Hearts were removed and placed in 5 mL of Iso buffer. Next, the heart tissue was passed through a motor-driven Potter–Elvehjem tissue grinder a total of five times. The homogenate was spun at 500 X *g* for 5 min at 4°C and the supernatant passed through a cheesecloth. Samples were then centrifuged at 5000 X *g* for 10 min. The resulting mitochondrial pellet was resuspended in 60 μL of Iso buffer. The protein concentration was determined by the BCA (bicinchoninic acid) method (Thermo Scientific) with a BSA as the standard.

Mitochondrial respiration measurements

Isolated mitochondria were diluted to 0.25 mg/mL in 210 mM mannitol, 70 mM sucrose, 10 mM MOPS, 5.0 mM KH_2PO_4, and 0.5 mg/mL BSA, pH 7.4, containing either 0.1 mM pyruvate and 1.0 mM malate, 30 μM palmitoylcarnitine and 1.0 mM malate, or 10 mM glutamate and 1.0 mM malate, as indicated. Respiration was measured at 20°C using a fiber optic oxygen measurement system (Instech) that uses the fluorescence lifetime technique. State 3 respiration was induced by the addition of ADP (0.5 mM) at the 2-minute mark. It is important to note that a physiological concentration of pyruvate (0.1 mM) was used, as hyper-physiological concentrations of pyruvate can mask effects of endogenous regulatory mechanisms.

PDH activity assay

Pyruvate dehydrogenase activity was measured according to our standardized assay conditions.[20] Briefly, following isolation, cardiac mitochondria were diluted to 0.05 mg/mL in a buffer containing 25 mM MOPS and 0.05% Triton X-100 at pH 7.4. Solubilization of mitochondria with 0.05% Triton X-100 inhibits complex I of the respiratory chain, preventing the consumption of NADH.[64] PDH activity was measured spectrophotometrically (Agilent, 8452A) as the rate of NAD^+ reduction to NADH (340 nm, ϵ = 6200 M^{-1} cm^{-1}) upon the addition of 2.5 mM pyruvate, 0.1 mM CoASH, 0.2 mM thiamine pyrophosphate, 1.0 mM NAD^+, and 5.0 mM $MgCl_2$ at pH 7.4.

NADH oxidase/complex I activity assay

NADH oxidase activity was measured as an overall assessment of electron transport chain activity through complexes I–III–IV. Once frozen-thawed isolated cardiac mitochondria were diluted into 25 mM MOPS (pH 7.4) at 0.01 mg/mL and the rotenone-sensitive rate of NADH oxidation was monitored spectrophotometrically utilizing an Agilent 8453 diode array UV—Vis spectrophotometer. Activity was measured as the rate of NADH oxidation (ε_{340} = 6200 M^{-1} cm^{-1}) following addition of 150 μM NADH. Complex I activity was measured spectrophotometrically as the rate of NADH oxidation in the presence of 50 nM antimycin A and 100 μM ubiquinone-1 following the addition of 150 μM NADH. Activity required the presence of ubiquinone-1 and was inhibited by rotenone (100 nM), indicating that NADH utilization was dependent on complex I activity.

CPT1 activity assay

CPT1 activity was measured in frozen total heart homogenates.[65] Samples were centrifuged 1000 X *g* for 5 min at 4°C. Protein concentration was determined using the BCA (bicinchoninic acid) method (Thermo Scientific) with BSA as the standard. Assay buffer was prepared using 25 mM MOPS, pH 7.4, 1 mM EGTA, and BSA (0.1%). Palmitoyl-CoA (100 μμM final), DTNB (100 μM final), and homogenate (1 μg/μL final) were then added. Samples were then mixed and incubated for 20 min at 20°C. CPT1 activity was measured spectrophotometrically (Agilent, 8452A) as the rate of increase at 412nm upon the addition of carnitine (10 mM final). Each set was run in triplicate and with the inclusion of one sample assayed without carnitine, which was subsequently used to subtract the background, carnitine-independent, activity.

Cardiac glycogen and protein carbonyl assay

Cardiac glycogen content was measured using a glycogen assay kit according to manufacturer's protocol (Sigma). Units were calculated using molecular weight of 180.16 g/mol. Protein Carbonyl content was assessed using a protein carbonyl assay kit according to manufacturer's protocol and ~45 mg tissue was utilized (abcam; ab126287).

Hepatic triglyceride assay

Liver samples (~100 mg tissue) were homogenized on ice for 60 s in 10X (v/w) Cell Signaling Lysis Buffer (Cell Signaling, Danvers, MA) with protease and phosphatase inhibitors (Boston BioProducts, Boston, MA). Total lipid was extracted from the homogenate using the Folch method with a 2:1 chloroform-methanol mixture.[66] Lipid was dried down using a nitrogen drier at room temperature, and resuspended in 200 μL of 3:1:1 *tert*-butyl alcohol-methanol-Triton X-100 solution. Final triglyceride concentrations were determined using a spectrophotometric assay with a 4:1 Free Glycerol Agent/Triglyceride Agent solution (Sigma Triglyceride; Free-Glycerol reagents, St. Louis, MO).[67]

Proteomic analysis

All samples were digested in gel using our standard methods.[20] Briefly, 20 μg samples were immobilized in a short run 12.5% SDS-PAGE gel (Criterion, Bio-rad), fixed and stained with Coomassie blue (Pierce). Each lane of the gel was cut as a single sample (~1mm^3 pieces), cut into smaller pieces, and washed/de-stained. The proteins were then reduced, alkylated, and digested with trypsin. Peptides were extracted with 70% methanol/5% acetic acid in water and the extracts were dried and reconstituted in 1% acetic acid. Samples were analyzed using our TSQ Quantiva system (Thermo Scientific). The HPLC was an Ultimate 3000 nano-flow system with a 10 cm × 75 μm i.d. C18 reversed phase capillary column which was packed in our laboratory in a New Objective Picofrit tip with a 10μm tip opening. The packing material was Phenomenex Aeris 3.6μm Peptide XB-C18 100A. Aliquots of 5μL were injected and the loading phase transferring the sample from the injection loop to the column at 1.25μL/min for 10min. The peptide eluted with a 60-minute gradient of acetonitrile in 0.1% formic acid. Data were acquired in the selected reaction monitoring (SRM) mode for our standard targeted quantitative proteomics panels.[68–70] Additional data was also acquired using high resolution accurate mass (HRAM) for potential re-interrogation in the future as needed. Data were analyzed using our established Skyline methods.[71] Protein abundance was determined by normalization to BSA used as a nonendogenous internal standard. Housekeeping proteins (Hspd1, Mdh1, Gpi1) were also used for normalization. The methods for proteomics assay development and data processing were performed according to our standard protocol.[20]

Metabolomic analysis

Tissue samples (~20 mg/each) was homogenized in 200 μL MeOH:PBS (4:1, v:v, containing 1,810.5 μM $^{13}C_3$-lactate and 142 μM $^{13}C_5$-glutamic acid) utilizing a Bullet Blender homogenizer (Next Advance, Averill Park, NY) in Eppendorf tubes. Next, 800 μL MeOH:PBS (4:1, v:v, containing 1,810.5 μM $^{13}C_3$-lactate and 142 μM $^{13}C_5$-glutamic acid) was added to samples and vortexed for 10 seconds and then stored at −20°C for 30 minutes. Samples were then sonicated in an ice bath for 30 minutes and subsequently centrifuged at 14,000 RPM for 10 minutes at 4°C. 800 μL of supernatant were transferred to a new Eppendorf tube. The samples were dried under vacuum using a CentriVap Concentrator (Labconco, Fort Scott, KS). Prior to MS analysis, the obtained residue was reconstituted in 150 μL 40% PBS/60% ACN. A quality control (QC) sample was made from all the study samples. The targeted LC-MS/MS method used here was modeled after that developed and used in a growing number of studies.[72–78] Analysis was performed using an Agilent 1290 UPLC-6490 QQQ-MS (Santa Clara, CA) system.

Samples (10 μL) were individually injected twice, for analysis on negative ionization mode and 4 μL was used for analysis on positive ionization mode. Chromatographic separations were done in hydrophilic interaction chromatography (HILIC) mode on a Waters XBridge BEH Amide column (150 × 2.1 mm, 2.5 μm particle size, Waters Corporation, Milford, MA). The flow rate was 0.3 mL/min with the auto-sampler kept at 4 C and the column compartment at 40 C. The mobile phase was composed of solvent A (10 mM ammonium acetate, 10 mM ammonium hydroxide in 95% H_2O/5% ACN) and solvent B (10 mM ammonium acetate, 10 mM ammonium hydroxide in 95% ACN/5% H_2O). Following the initial 1 min isocratic elution of 90% Solvent B, the percentage of solvent B was reduced to 40% at t = 11 min. Solvent B was maintained at 40% for 4 min (t = 15 min) then increased gradually back to 90%, to prepare for the next injection. The mass spectrometer is equipped with an electrospray ionization (ESI) source. Targeted data acquisition was performed in multiple-reaction-monitoring (MRM) mode. The LC-MS/MS system utilized Agilent MassHunter Workstation software (Santa Clara, CA). The extracted MRM peaks were integrated using Agilent MassHunter Quantitative Data Analysis (Santa Clara, CA). Acetonitrile (ACN), methanol (MeOH), ammonium acetate, and acetic acid obtained from Fisher Scientific (Pittsburgh, PA). Ammonium hydroxide from Sigma-Aldrich (Saint Louis, MO). DI water was used with the EMD Millipore Water Purification System (Billerica, MA). PBS from GE Healthcare Life Sciences (Logan, UT). The standard compounds corresponding to the

measured metabolites were purchased from Sigma-Aldrich (Saint Louis, MO) and Fisher Scientific (Pittsburgh, PA).

Western blot analysis

Fresh heart tissue was resuspended in Iso buffer and homogenized as described in the "Isolation of Cardiac Mitochondria" methods above. Homogenates were next centrifuged for 5 min at 500 *g*, and supernatants were diluted with 4x NuPAGE sample buffer (Invitrogen) containing 25 mM DTT and heated at 95°C for 5 min. Western blot was performed following Li-COR manufacturer's protocol Following SDS-PAGE (4–12% NuPAGE BisTris gel, Thermo Fisher Scientific), gels were transferred to nitrocellulose membranes and blocked for 60 min with Odyssey TBS blocking buffer (LI- COR) at room temperature. For the indicated Western blots, intensities of bands were standardized to the total protein loaded (Revert Total Protein Stain; LI-COR, 926–11014). Antibodies used for these experiments were as follows: PDH, pPDH, ACC, pACC, 4E-BP1, p4E-BP1, and Akt, pAkt (Cell Signaling product nos. 3205, 31866, 3676, 11818, 9452, 2855, 4685, and 31957, respectively). Antibodies were diluted 1:2000 in block buffer added overnight at 4°C and subsequently washed the following day, and the secondary antibody (IRDye 800CW, LI-COR; 1:10,000 dilution) was incubated for 1 h. Following additional washing, blots were analyzed on an Odyssey CLx imaging system using Image Studio software (LI-COR).

Figure design

The graphical abstract along with Figures 4 and 5 were created using Biorender.com

QUANTIFICATION AND STATISTICAL ANALYSIS

Statistical details of experiments can be found in the figure legends, including the statistical test used, exact value of n, definition of center, and dispersion and precision measures. Data were analyzed using GraphPad Prism 9. Pairwise comparison between groups was performed using a paired or unpaired two-tailed Student's *t* test, as specified. Multiple comparison was performed using 2-way ANOVA with Tukey post hoc analysis, unless otherwise noted. $p < 0.05$ was considered statistically significant. Data are presented as means with SD.

Statistical details for -omics datasets

For metabolomics data, the relative abundance of annotated metabolites was calculated by peak area and normalized per tissue weight and internal standards. The data were then Log-transformed and subjected to 2-way ANOVA, and Student's *t*-tests. 2-way ANOVA was used to decrease the number of repetitive Student's *t*-tests. For this, all metabolites that did not pass a significance threshold ($p < 0.05$) for both factors (sex and diet) were excluded from the further Student's *t*-tests to reduce the probability of false positive outcomes. MHT correction was not utilized as the goal was to explore the data on interaction effect and reduced the number of repetitive tests. In the following downstream individual *t*-tests $q < 0.05$ after Benjamini-Hochberg FDR correction as significance threshold was used. The pathway analysis of the metabolomics (via MetaboAnalyst) and proteomics data (via STRING) was performed over KEGG database and used $q < 0.05$ as significance threshold.[79,80] Cluster analysis, heatmap visualization in statistical procedures were performed under R-environment [www.r-project.org].